




Review

# Recent Achievements in Development of TiO<sub>2</sub>-Based Composite Photocatalytic Materials for Solar Driven Water Purification and Water Splitting

Klara Perović<sup>1,†</sup>, Francis M. dela Rosa<sup>1,†</sup>, Marin Kovačić<sup>1</sup> , Hrvoje Kušić<sup>1,\*</sup>,  
Urška Lavrenčič Štanger<sup>2</sup> , Fernando Fresno<sup>3</sup>, Dionysios D. Dionysiou<sup>4</sup>  and  
Ana Lončarić Božić<sup>1</sup>

<sup>1</sup> Faculty of Chemical Engineering and Technology, University of Zagreb, Marulicev trg 19, HR-10000 Zagreb, Croatia; kperovic@fkit.hr (K.P.); frosa@fkit.hr (F.M.d.R.); mkovacic@fkit.hr (M.K.); abozic@fkit.hr (A.L.B.)

<sup>2</sup> Faculty of Chemistry and Chemical Technology, University of Ljubljana, 1000 Ljubljana, Slovenia; Urška.Lavrencic.Stanger@fkkt.uni-lj.si

<sup>3</sup> Photoactivated Processes Unit, IMDEA Energy, Móstoles, 28935 Madrid, Spain; fernando.fresno@imdea.org

<sup>4</sup> Environmental Engineering and Science Program, University of Cincinnati, Cincinnati, OH 45221-0012, USA; DIONYSDD@UCMAIL.UC.EDU

\* Correspondence: hkusic@fkit.hr

† Equal contribution.

Received: 3 February 2020; Accepted: 11 March 2020; Published: 15 March 2020



**Abstract:** Clean water and the increased use of renewable energy are considered to be two of the main goals in the effort to achieve a sustainable living environment. The fulfillment of these goals may include the use of solar-driven photocatalytic processes that are found to be quite effective in water purification, as well as hydrogen generation. H<sub>2</sub> production by water splitting and photocatalytic degradation of organic pollutants in water both rely on the formation of electron/hole ( $e^-/h^+$ ) pairs at a semiconducting material upon its excitation by light with sufficient photon energy. Most of the photocatalytic studies involve the use of TiO<sub>2</sub> and well-suited model compounds, either as sacrificial agents or pollutants. However, the wider application of this technology requires the harvesting of a broader spectrum of solar irradiation and the suppression of the recombination of photogenerated charge carriers. These limitations can be overcome by the use of different strategies, among which the focus is put on the creation of heterojunctions with another narrow bandgap semiconductor, which can provide high response in the visible light region. In this review paper, we report the most recent advances in the application of TiO<sub>2</sub> based heterojunction (semiconductor-semiconductor) composites for photocatalytic water treatment and water splitting. This review article is subdivided into two major parts, namely Photocatalytic water treatment and Photocatalytic water splitting, to give a thorough examination of all achieved progress. The first part provides an overview on photocatalytic degradation mechanism principles, followed by the most recent applications for photocatalytic degradation and mineralization of contaminants of emerging concern (CEC), such as pharmaceuticals and pesticides with a critical insight into removal mechanism, while the second part focuses on fabrication of TiO<sub>2</sub>-based heterojunctions with carbon-based materials, transition metal oxides, transition metal chalcogenides, and multiple composites that were made of three or more semiconductor materials for photocatalytic water splitting.

**Keywords:** TiO<sub>2</sub> heterojunction; semiconductor coupling; water treatment; photocatalytic degradation; photocatalytic water splitting; H<sub>2</sub> production

## 1. Introduction

Nowadays, accessible clean water and energy resources are among the highest priorities for sustainable economic growth and societal wellbeing. Water supports life and is a crucial resource for humanity; it is also at the core of natural ecosystems and climate regulation. Water stress is primarily a water quantity issue, but it also occurs as a consequence of a deterioration of water quality and a lack of appropriate water management [1]. Environmental problems that are associated with water pollution have been a persistently important issue over recent decades, correlated negatively with the health and ecosystem. Activities of the Water JPI's *Strategic Research and Innovation Agenda* focus on, among others, new materials and processes, energy efficiency, thus supporting key enabling technologies for clean water and wastewater treatment [2]. *EU Energy Strategies 2020, 2030, and 2050* set increasing standards for the reduction of greenhouse gas emissions by 20, 40, and 80–95%, respectively, which is achievable by significant investments in the development and application of new low-carbon and renewable energy technologies [3]. In light of increased energy demands and the need to reduce greenhouse gas emissions, the focus has been turned from the fossil fuels toward renewable energy resources and vectors: solar, wind, tides, waves, geothermal, biomass, biofuels, and hydrogen (H<sub>2</sub>) [4]. Alternative fuels are required to have as small environmental footprint, and be storable and economical, whereas H<sub>2</sub> satisfies the first two conditions. The research over the last decades has been focused on fulfilling the third requirement, which triggers its production by solar energy, a largely available and intrinsically renewable energy resource, through water splitting. It should be emphasized that H<sub>2</sub>, as a fuel, possesses higher heat content than gasoline (per unit mass) [5].

The pioneering work of Fujishima and Honda [6] for H<sub>2</sub> production by photoelectrochemical water splitting while using TiO<sub>2</sub> photoanode and Pt cathode opened the potential possibilities for generating this energy vector, i.e., fuel, directly from water and solar energy. Works by Bard and Frank in 1977 [7], exhibiting photocatalytic oxidation of CN to CNO<sup>-</sup>, and by Ollis et al. [8], studying the photocatalytic degradation of organic contaminants in water, practically opened a new research field within new water purification technologies. H<sub>2</sub> production by water splitting and photocatalytic degradation of organic pollutants in water both rely on the formation of electron/hole ( $e^-/h^+$ ) pairs at a semiconducting material upon its excitation by light with sufficient photon energy [9–12]. These processes, which can be conducted under environmentally friendly and mild conditions, are economically viable, possessing a potential of becoming effective methods to produce clean energy and water, owing to their low-cost, long-term stability, and usage of solar energy [13].

A well-suited model catalyst for photocatalytic studies is TiO<sub>2</sub>. Its wide application has been promoted, due to: (i) high photocatalytic activity under the incident photon wavelength of  $300 < \lambda < 390$  nm and (ii) multi-faceted functional properties, such as chemical and thermal stability, resistance to chemical breakdown, and attractive mechanical properties [14,15]. However, harvesting a broader spectrum of solar irradiation involves the lowering of the band gap of semiconducting material, whilst inhibiting the recombination of photogenerated charges. Strategies, including doping with non-metals, incorporation or deposition of noble metals (ions), and material engineering solutions that are based on composites formation using transition metals, carbon nanotubes, dye sensitizers, conductive polymers, graphene (oxide), and semiconducting materials, present viable solutions for set tasks [9,10,15,16]. It is of great importance to combine TiO<sub>2</sub> with narrow band gap semiconductors with visible light response to obtain an effective composite for photocatalytic applications. The obtained synergistic effect between two or more semiconductors will then promote efficient charge separation, sufficient visible light response, and high photocatalytic performance. With the dramatic increase of the papers published related to these topics, a comprehensive review is desirable, providing a general overview on processes occurring while using TiO<sub>2</sub>-based heterojunction (semiconductor) systems for photocatalytic water purification and water splitting. Despite reviews focusing on TiO<sub>2</sub>-based semiconductor composites [17,18], those focusing on the removal of contaminants of emerging concern (CECs) are quite scarce. In addition, this review also summarizes TiO<sub>2</sub>-based nanocomposites for photocatalytic water splitting providing insight into effectiveness of a variety of materials groups representing the

alternative for replacing the utilization of expensive, toxic, and non-abundant materials. The first part of the review focuses on TiO<sub>2</sub>-based heterojunction (semiconductor-semiconductor coupling) composites, being selected on the basis of band gap energies suitable to make heterojunctions with documented applications providing promising results in CECs treatment and stability of prepared materials, and also respecting their most recent applications for the photocatalytic degradation of CECs (i.e., demonstrating the current focus within the field), such as pharmaceuticals and pesticides, with critical insight into the pollutants removal mechanism. The second part targets the most recent achievements in the field of fabrication of TiO<sub>2</sub>-based heterojunctions with carbon based materials, transition metal oxides, transition metal chalcogenides, and multiple composites that were made of three or more semiconductor materials for photocatalytic water splitting.

## 2. Photocatalytic Water Treatment

The general mechanism of semiconductor photocatalysis (Figure 1) is composed of three main steps: 1.  $e^-/h^+$  pairs are generated on the surface of the semiconductor under illumination with the required wavelength or energy; then, 2.) photogenerated charges (i.e.,  $e^-/h^+$ ) migrate to the surface of the semiconductor; and lastly, 3.)  $e^-$  and  $h^+$  induce redox reactions on the surface that facilitate destruction of organic pollutants [19,20]. As stressed above, TiO<sub>2</sub> is still the most studied and widely used material for photocatalytic degradation reactions. However, TiO<sub>2</sub> suffers from fast  $e^-/h^+$  pair recombination and large band gap ( $E_g = 3.1\text{--}3.2$  eV), which can only be excited under UV light irradiation. The strategies for improving these issues are provided above, while, among them, semiconductor-coupling presents a viable structure-properties engineering solution for the enhancement of TiO<sub>2</sub> photocatalytic activity due to the simultaneously reduced  $e^-/h^+$  recombination rate and enhanced visible light absorption [21].

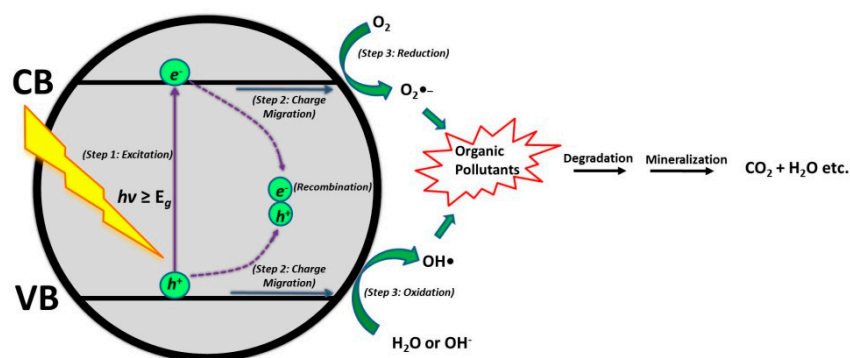


Figure 1. Photocatalytic reaction mechanism over semiconductor material.

Three main types of heterojunction architectures are reported for TiO<sub>2</sub>/semiconductor composites [22]. In Type I heterojunction, the conduction band (CB) of TiO<sub>2</sub> is higher in energy (more negative potential) when compared to the CB of semiconductor 2 and the valence band (VB) of TiO<sub>2</sub> is lower in energy (more positive potential) as compared to the VB of semiconductor 2 [23,24]. This leads to the accumulation of photogenerated  $h^+$  and  $e^-$  in semiconductor 2. In Type II heterojunction (where TiO<sub>2</sub> can be semiconductor 1 or 2), the CB of semiconductor 2 is higher than the CB position of semiconductor 1 leading to facile transfer of photogenerated  $e^-$  from CB of semiconductor 2 to CB of semiconductor 1 [25]. Meanwhile, photogenerated  $h^+$  in VB of semiconductor 1 can travel to the VB of semiconductor 2, which facilitates efficient charge separation. Type III heterojunction (also known as broken gap situations) [26] shares the same charge transfer mechanism, like Type II heterojunction. In this case, the CB and VB of semiconductor 2 are higher than CB and VB of TiO<sub>2</sub> [27,28]. These heterojunction types are explained in detail in the context of particular material combinations in the further text and graphically represented through Figures 2, 3 and 5–10.

## 2.1. Coupling of TiO<sub>2</sub> with Metal Oxides

### 2.1.1. TiO<sub>2</sub>/WO<sub>3</sub>

Tungsten oxide (WO<sub>3</sub>), which is a visible light active photocatalyst with band gap of 2.4–2.8 eV, is a promising candidate for photocatalytic applications, due to its oxidative properties, nontoxicity, low cost, and stability in acidic solutions. In addition, WO<sub>3</sub> directly matches the band positions of TiO<sub>2</sub> to form a heterojunction (*Type II Heterojunction*) [29–32]. Several authors studied the application of TiO<sub>2</sub>/WO<sub>3</sub> composites for the degradation of various CECs; either pesticides or pharmaceuticals (Table 1). Hence, Macias et al. [24] studied the photocatalytic degradation of herbicide 2,4-dichlorophenoxyacetic acid (2,4-D) while using TiO<sub>2</sub>/WO<sub>3</sub> composites under natural sunlight. They reported the rather high effectiveness of the studied system: 94.6% degradation of 2,4-D and 88.6% mineralization of overall organic content under two and four hours of natural sunlight irradiation, respectively.

Besides, they studied the mechanisms that are responsible for forming reactive species within the system and, based on their findings, proposed that, upon forming  $e^-/h^+$  pairs under solar irradiation, photogenerated  $e^-$  from CB of TiO<sub>2</sub> are transferred to CB of WO<sub>3</sub>. Consequently, W<sup>6+</sup> was first reduced to W<sup>5+</sup> on WO<sub>3</sub> surface, while the W<sup>5+</sup> ions are then oxidized to W<sup>6+</sup> by adsorbed O<sub>2</sub> producing superoxide anion radical (O<sub>2</sub><sup>•-</sup>). The photogenerated  $h^+$  in VB of WO<sub>3</sub> are transferred to VB of TiO<sub>2</sub> where they reacted with water (or hydroxyl ions, HO<sup>-</sup>) forming hydroxyl radicals (•OH) (Figure 2). The generated reactive oxygen species (ROS) promoted the degradation of 2,4-D and its intermediates, eventually yielding rather high mineralization extents, while their occurrence in the system was confirmed through tests with common scavenging agents (e.g., tert-butanol (TB) for •OH, formic acid (FA) for  $h^+$ , and *p*-benzoquinone (BQ) for O<sub>2</sub><sup>•-</sup>) [24].

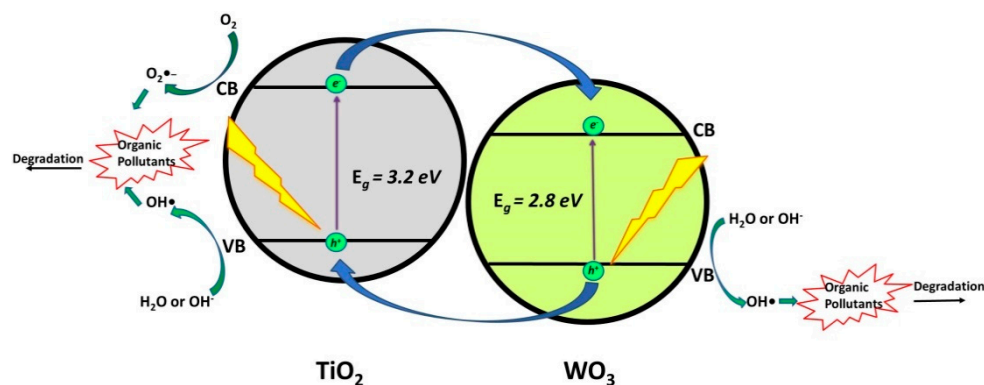


Figure 2. Photocatalytic degradation mechanism over TiO<sub>2</sub>/WO<sub>3</sub> composite.

The same composite type was used in the degradation of pharmaceuticals. Hence, Mugunthan et al. [30] treated diclofenac (DCF) while using TiO<sub>2</sub>/WO<sub>3</sub> composites under 4 hrs of visible light irradiation and reported a maximum of 92% mineralization of overall organic content. They also elucidated the DCF degradation pathway by LC/MS measurements, which included C-N cleavage in the DCF molecule forming benzene-ring based intermediates at the first stage, and open-ring intermediates at the later stage, which were eventually mineralized. Such findings were quite similar to other studies employing •OH based processes in the degradation of DCF ([33,34]), thus implying the important role of formed ROS, primarily •OH, in the case of TiO<sub>2</sub>/WO<sub>3</sub> solar driven photocatalysis as well. Arce-Sarria et al. [35] studied the performance of TiO<sub>2</sub>/WO<sub>3</sub> composite for the degradation of another pharmaceutical, Amoxicillin (AMX), in pilot scale reactor, where they achieved 64.4% degradation.

**Table 1.** Photocatalytic degradation of contaminants of emerging concern (CECs) over TiO<sub>2</sub>/WO<sub>3</sub> composites.

Catalyst	Target Pollutant	Initial Concentration/Working Volume ((mg L <sup>-1</sup> )/mL)	Experimental Conditions	Reaction Time	Removal Extent (%)	Reference
TiO <sub>2</sub> - WO <sub>3</sub> (0.5 g/L)	2,4-dichlorophenoxy acetic acid	50 (in 250 mL)	Light Source: natural sunlight 11AM-4PM; pH = 4	120 min	94.6 (TOC = 88.6)	[24]
TiO <sub>2</sub> - WO <sub>3</sub> (0.6 g/L)	Diclofenac	25 (in 100 mL)	Light Source: 400 W Metal Halide Lamp; pH = 5	240 min	TOC = 91	[30]
TiO <sub>2</sub> - WO <sub>3</sub> (0.1 g/L)	Amoxicillin	100 (in 25,000 mL)	CPC Reactor with accumulated energy 550,000 J/m <sup>2</sup>	NA	64.4 (@ 550 kJ/m <sup>2</sup> )	[35]
(WO <sub>3</sub> /TiO <sub>2</sub> -C) (1.0 g/L)	Diclofenac	10 (in 300 mL)	Light Source: 1500 W Xenon Lamp with filter( $\lambda > 290$ nm) ; pH = 7	NA	100 (@ 250 kJ/m <sup>2</sup> ) (TOC = 82.4 @ 400 kJ/m <sup>2</sup> )	[32]
(WO <sub>3</sub> /TiO <sub>2</sub> -N) (1.0 g/L)	Diclofenac	10	Light Source: 1500 W Xenon Lamp with ID65 solar filter; pH = 6.5	NA	100 (@ 250 kJ/m <sup>2</sup> ) (TOC = 100 @400 kJ/m <sup>2</sup> )	[31]

NA—not available.

Besides “pure” TiO<sub>2</sub>/WO<sub>3</sub> composite, several authors studied the performance of its enriched analogues (Table 1). Hence, Cordero-García et al. [32] studied DCF degradation by WO<sub>3</sub>/C-doped TiO<sub>2</sub> and reported 100% DCF degradation and 82.4% mineralization of the overall organic content under 250 kJ/m<sup>2</sup> and 400 kJ/m<sup>2</sup> of solar-accumulated energy, respectively. They also stated that the WO<sub>3</sub>/C-doped TiO<sub>2</sub> composite showed superior photocatalytic activity for the complete degradation and mineralization of DCF when comparing to the pristine TiO<sub>2</sub>, used as benchmark material. Based on the findings on elucidated mechanisms within the studied composite and DCF degradation pathway provided, the authors concluded that the incorporation of elemental carbon to TiO<sub>2</sub> crystal structure promoted the formation of a C2p-hybridized valence band that lowered the band gap of TiO<sub>2</sub> by mixing with O2p orbitals. As a result, upon visible light irradiation, TiO<sub>2</sub> generates  $e^-/h^+$  pairs, where the photogenerated  $e^-$  are promoted to the Ti 3d states (VB), thus reducing Ti<sup>4+</sup> to Ti<sup>3+</sup>. Ti<sup>3+</sup> can be easily oxidized by WO<sub>3</sub> due to the differences in the reduction potential between TiO<sub>2</sub> (−0.70 V vs NHE) and WO<sub>3</sub> (−0.03 V vs NHE). Subsequently, W<sup>6+</sup> traps photogenerated  $e^-$  to form its reduced state W<sup>5+</sup>, while the redox reaction occurs further by returning to its original oxidation state in reaction with adsorbed O<sub>2</sub> on the composite catalyst surface (similarly as discussed above in the case of “pure” TiO<sub>2</sub>/WO<sub>3</sub>), thus leading to improved charge separation and the formation of ROS, which contributed in DCF degradation and mineralization of formed intermediates. The same authors studied the degradation of DCF with another enhanced WO<sub>3</sub>/TiO<sub>2</sub> composite (N-doped TiO<sub>2</sub>), and again reported high degradation and mineralization rates; 100% according to both indicators under 250 kJ/m<sup>2</sup> and 400 kJ/m<sup>2</sup> of solar-accumulated energy, respectively [31]. They stressed that the same mechanism that was responsible for the enhancement of photocatalyst activity in C-doped WO<sub>3</sub>/TiO<sub>2</sub> composite [32] also improved the performance of N-doped WO<sub>3</sub>/TiO<sub>2</sub> [31].

### 2.1.2. TiO<sub>2</sub>/Fe<sub>2</sub>O<sub>3</sub>

Iron oxide ( $\alpha$ -Fe<sub>2</sub>O<sub>3</sub>) is a promising candidate for photocatalytic applications, due to its abundance, nontoxicity, low cost, stability in aqueous solutions (pH > 3), and narrow band gap (2.0–2.2 eV), which directly matches the band positions of TiO<sub>2</sub> to form heterojunction (*Type I Heterojunction*) [23,36].

Several authors report the photocatalytic degradation of CECs using TiO<sub>2</sub>/Fe<sub>2</sub>O<sub>3</sub> composites (Table 2). Hence, Mirmasoomi et al. [37] used TiO<sub>2</sub>/Fe<sub>2</sub>O<sub>3</sub> as a catalyst for photocatalytic degradation of Diazinon (DZ). The authors reported an optimized system with maximum degradation of DZ equal to 95.07% within 45 min. under visible light irradiation. In another study by Moniz et al. [23], photocatalytic degradation of 2,4-D while using TiO<sub>2</sub>/Fe<sub>2</sub>O<sub>3</sub> composites was investigated, reporting 100% 2,4-D degradation and 100% mineralization of overall organic content within 2 h and 3 h, respectively, using irradiation from a 300 W Xenon Lamp. The authors found out that, when compared to the benchmark TiO<sub>2</sub> (P25), the TiO<sub>2</sub>/Fe<sub>2</sub>O<sub>3</sub> composite shows superior photocatalytic activity. Based on photoluminescence and photocurrent studies, the TiO<sub>2</sub>/Fe<sub>2</sub>O<sub>3</sub> composite exhibits enhanced separation of  $e^-/h^+$  pairs due to the formed heterojunction. The proposed mechanism was supported with DFT studies, which firstly involved the transfer of photogenerated  $e^-$  from TiO<sub>2</sub> CB to Fe<sub>2</sub>O<sub>3</sub> CB. In addition, Fe<sub>2</sub>O<sub>3</sub> binds strongly with (dissolved) oxygen, thus aiding the photoelectron transfer. This *in-situ* second stage mechanism facilitates the facile migration of  $h^+$  from the VB of TiO<sub>2</sub> [23]. Macías et al. [24] studied the same system, TiO<sub>2</sub>/Fe<sub>2</sub>O<sub>3</sub> composites for photocatalytic degradation of 2,4-D, but while using natural sunlight. The authors reported 96.8% 2,4-D degradation and 90.0% mineralization of overall organic content under two hours and four hours, respectively. Contrary to the presented mechanism of Moniz et al. [23], Macias et al. [24] proposed that the incorporation of Fe<sub>2</sub>O<sub>3</sub> causes the photogenerated  $e^-$  in CB of TiO<sub>2</sub> to be transferred to CB of Fe<sub>2</sub>O<sub>3</sub>, promoting the reduction of Fe<sup>3+</sup> to Fe<sup>2+</sup>. Photogenerated  $h^+$  in VB of TiO<sub>2</sub> are transferred to VB of Fe<sub>2</sub>O<sub>3</sub>, which leads to the regeneration of Fe<sup>3+</sup> and avoids the recombination of  $e^-/h^+$  pairs at TiO<sub>2</sub> surface. In addition, Fe<sub>2</sub>O<sub>3</sub> ( $E_g = 2.2$  eV) can be excited by visible light irradiation producing photogenerated  $e^-/h^+$  pairs. Photogenerated  $e^-$  in CB of Fe<sub>2</sub>O<sub>3</sub> can be transferred to O<sub>2</sub> dissolved in water to form O<sub>2</sub><sup>•−</sup>, while photogenerated  $h^+$  in VB of Fe<sub>2</sub>O<sub>3</sub> can facilitate generation of •OH eventually contributing to the degradation of present organics [24] (Figure 3). The formation of mentioned ROS and their involvement in degradation of targeted pollutant was confirmed through common scavenging tests using TB, FA, and BQ.

**Table 2.** Photocatalytic degradation of CEC's over TiO<sub>2</sub>/Fe<sub>2</sub>O<sub>3</sub> composites.

Catalyst	Target Pollutant	Initial Concentration/Working Volume ((mg L <sup>-1</sup> )/mL)	Experimental Conditions	Reaction Time	Removal Extent (%)	Reference
TiO <sub>2</sub> /Fe <sub>2</sub> O <sub>3</sub> (0.1 g/L)	Diazinon	10 (in 300 mL)	Light Source: 60 W Philips Visible lamp; pH = natural	45 min	95.07	[37]
TiO <sub>2</sub> /Fe <sub>2</sub> O <sub>3</sub> (10 mg)	2,4-dichlorophenoxy acetic acid	50 (in 100 mL)	Light Source: 300 W Xenon Lamp; pH = natural	120 min	100 (TOC = 100 @ 150 min.)	[23]
TiO <sub>2</sub> /Fe <sub>2</sub> O <sub>3</sub> (0.5 g/L)	2,4-dichlorophenoxy acetic acid	50 (in 250 mL)	Light Source: natural sunlight 11AM-4PM; pH = 4	120 min	96.8 (TOC =90 @ 240 min.)	[24]
TiO <sub>2</sub> /Fe <sub>2</sub> O <sub>3</sub> (70 mg)	Oxytetracycline Hydrochloride	60 (in 70 mL)	Light Source: 300 W Iodine Tungsten Lamp; pH = 5.5	300 min	75.6	[38]
TiO <sub>2</sub> /Fe <sub>2</sub> O <sub>3</sub> (1.0 g/L)	Oxytetracycline	60	Light Source: 300 W Iodine Tungsten Lamp; pH = 5.5	300 min	~80	[39]
TiO <sub>2</sub> /Fe <sub>2</sub> O <sub>3</sub> /CNT (100 mg)	Tetracycline	20 (in 100mL)	Light Source: 300 W Xenon Lamp; pH = natural	90 min	89.41	[40]
TiO <sub>2</sub> -coated α-Fe <sub>2</sub> O <sub>3</sub> core-shell (100 mg)	Tetracycline Hydrochloride	50 (in 200 mL)	Light Source: 300 W Xenon Lamp (λ > 420 nm) ; pH = 5. 45 Oxidant = 120 μL (30% H <sub>2</sub> O <sub>2</sub> )	90 min	100	[41]

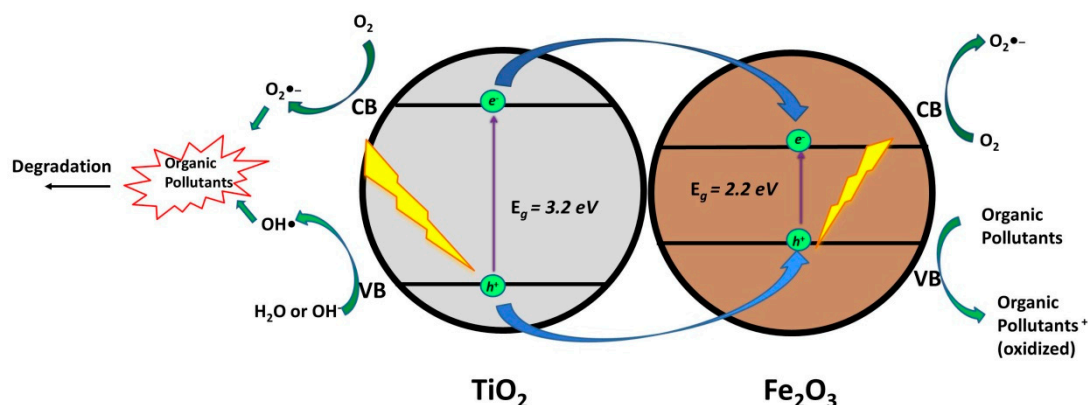


Figure 3. Photocatalytic degradation mechanism over  $\text{TiO}_2/\text{Fe}_2\text{O}_3$  composite.

The photocatalytic degradation of the pharmaceutical tetracycline (TC) and its derivatives, such as oxytetracycline (OTC), using  $\text{TiO}_2/\text{Fe}_2\text{O}_3$  materials has also been reported. Hence, it was found out that, under visible light irradiation ( $\lambda = 400\text{--}750\text{ nm}$ ),  $\alpha\text{-Fe}_2\text{O}_3$  was activated and generated  $e^-/h^+$  pairs, and then photogenerated  $e^-$  from CB of  $\alpha\text{-Fe}_2\text{O}_3$  moved to  $\text{TiO}_2$  trapping sites for atmospheric  $\text{O}_2$  to form  $\text{O}_2^{\bullet-}$ , which was proven to largely contribute to the degradation of OTC. On the other hand, the photogenerated  $h^+$  from VB of  $\alpha\text{-Fe}_2\text{O}_3$  primarily reacted with  $\text{OH}^-$ , resulting in the generation of  $\bullet\text{OH}$ , which also contributed to the degradation of OTC. When compared to  $\text{TiO}_2$  reference material, the  $\text{TiO}_2/\text{Fe}_2\text{O}_3$  composite exhibited an enhanced photocatalytic activity under visible light due to efficient  $e^-/h^+$  separation, as stated above [38]. The same authors [38,39] also studied the degradation mechanism of OTC while using LC/MS TOF analysis and, based on the formed intermediates, established the OTC degradation pathway, and concluded that  $\bullet\text{OH}$  mainly mediated degradation. Besides, “pure”  $\text{TiO}_2/\text{Fe}_2\text{O}_3$ , enriched analogue with carbon nanotubes (CNTs) was also studied (Table 2). Hence,  $\text{TiO}_2/\text{Fe}_2\text{O}_3/\text{CNTs}$  was used as the catalyst for photocatalytic degradation of TC, under visible light illumination [40]. It was found that the effectiveness of photocatalytic degradation of TC within 90 min. treatment using  $\text{TiO}_2/\text{Fe}_2\text{O}_3/\text{CNTs}$  was almost twice higher when comparing to that achieved by benchmark  $\text{TiO}_2$ ; 89.41% and 47.64%, respectively. The authors attributed the improved photocatalytic efficiency to the presence of the CNT, which acted as a photogenerated  $e^-$  acceptor, thereby suppressing  $e^-/h^+$  recombination [40]. In another study, the core-shell structured  $\alpha\text{-Fe}_2\text{O}_3$  (with  $\text{TiO}_2$  shell of around 15 nm) exhibited 100% TC removal in 90 min. [41]. The degradation improvement was ascribed to the addition of  $\text{H}_2\text{O}_2$  in the system, which generated more ROS than by the common photocatalytic mechanisms described above [41]. Hence, the contribution of  $\text{H}_2\text{O}_2$  in such a system can be described through restraining  $e^-/h^+$  recombination and increasing  $\text{HO}\bullet$  generation in the system, as in Equation (1) [15]:



### 2.1.3. $\text{TiO}_2$ /Spinel Ferrite

Spinel ferrites ( $\text{MFe}_2\text{O}_4$ ) are metal oxides, where M is a divalent ion (i.e.,  $\text{Mg}^{2+}$ ,  $\text{Ca}^{2+}$ ,  $\text{Sr}^{2+}$ ,  $\text{Ni}^{2+}$ ,  $\text{Zn}^{2+}$ , etc.), serving as promising candidates for photocatalytic applications due to their narrow band gap range (1.3–2.2 eV) and magnetic properties [42,43]. Spinel ferrites band positions match  $\text{TiO}_2$ , thus possessing compatibility to form a heterojunction (*Type II Heterojunction*) [44–47].

The literature provides applications of  $\text{MFe}_2\text{O}_4/\text{TiO}_2$  materials as photocatalysts in treatment of CECs, as in the case of previously discussed  $\text{TiO}_2$ -based composites, however, it should be noted that authors within such composites used modified  $\text{TiO}_2$  (Table 3). Hence, Chen et al. [44] studied photocatalytic degradation of TC and its derivatives using N-doped  $\text{TiO}_2/\text{CaFe}_2\text{O}_4/\text{diatomite}$ , and reported 91.7% removal of TC within 150 min. under visible light irradiation. The authors studied the composite stability and reusability; the results obtained after five cycles indicates that employed



composite is rather stable, enabling 89.2% removal of TC. They also proposed the photocatalytic mechanism occurring within the composite; the excitation of both N-TiO<sub>2</sub> and CaFe<sub>2</sub>O<sub>4</sub> by visible light leads to the formation of  $e^-/h^+$  pairs (Figure 4). The photogenerated  $e^-$  in CB of N-TiO<sub>2</sub> can directly react to adsorbed O<sub>2</sub> generating O<sub>2</sub><sup>•-</sup>, while photogenerated  $h^+$  in VB of N-TiO<sub>2</sub> directly react with H<sub>2</sub>O and OH<sup>-</sup> producing •OH. Simultaneously, photogenerated  $e^-$  in CB of CaFe<sub>2</sub>O<sub>4</sub> can undergo the same mechanism (i.e., reaction with O<sub>2</sub> to produce O<sub>2</sub><sup>•-</sup>). In addition, the formed heterojunction helps the migration of  $e^-$  from CB of CaFe<sub>2</sub>O<sub>4</sub> to CB of N-TiO<sub>2</sub>, and  $h^+$  from VB of N-TiO<sub>2</sub> to VB of CaFe<sub>2</sub>O<sub>4</sub> (Figure 4). Such a transfer of charge carriers between the two semiconductors hinders the recombination process and enhances the photocatalytic activity of the composite, thus leading to more efficient generation of ROS (O<sub>2</sub><sup>•-</sup> and •OH) [44]; the existence of formed ROS was confirmed through scavenging tests while using isopropyl alcohol (IPA), ammonium oxalate (AO), and BQ for •OH,  $h^+$  and O<sub>2</sub><sup>•-</sup>, respectively. Such behavior is confirmed by studying the degradation pathway of TC; it was found that the TC intermediates match those that formed through radical driven reactions undergoing in the first step demethylation and hydroxylation. The second step considered the removal of functional groups (amino, hydroxyl, and methyl) and further ring opening reactions that are mainly mediated by photogenerated  $h^+$ , yielding small fragments that were eventually mineralized [44]. Such a pathway confirmed the dual role of photogenerated  $h^+$ , as a promotor •OH generation and as sites for the direct oxidation of adsorbed organics. There are several other studies investigating the application of different MFe<sub>2</sub>O<sub>4</sub>/TiO<sub>2</sub> materials (N-doped TiO<sub>2</sub>/SrFe<sub>2</sub>O<sub>4</sub> diatomite [46]; Ce/N-co-doped TiO<sub>2</sub>/NiFe<sub>2</sub>O<sub>4</sub>/ diatomite and ZnFe<sub>2</sub>O<sub>4</sub>/TiO<sub>2</sub> [47]) for the photocatalytic degradation of CECs, such as TC, OTC, and bisphenol A (BPA). Interestingly, the same mechanisms responsible for charge transfer and consequent generation of ROS were reported, regardless of the different M type within the spinel ferrite part of composite and/or TiO<sub>2</sub> (non-doped or doped with metal and/or non-metal ions).

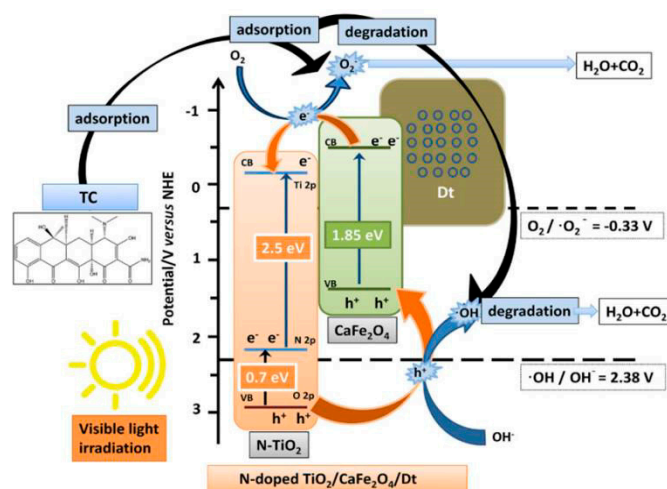


**Figure 4.** Proposed mechanism for the tetracycline (TC) photodegradation process using N-doped TiO<sub>2</sub>/CaFe<sub>2</sub>O<sub>4</sub>/ diatomite [44].

**Table 3.** Photocatalytic degradation of CEC's over TiO<sub>2</sub>/MFe<sub>2</sub>O<sub>4</sub> composites.

Catalyst	Target Pollutant	Initial Concentration/ Working Volume ( $\text{mg L}^{-1}$ )/mL)	Experimental Conditions	Reaction Time	Removal Extent (%)	reference
N-TiO <sub>2</sub> / CaFe <sub>2</sub> O <sub>4</sub> /diatomite (2.0 g/L)	Tetracycline	10 (in 200 mL)	Light Source: 150 W Xenon Lamp with UV light filter	150 min	91.7 (TOC = ~80 @ 2h)	[44]
N-TiO <sub>2</sub> / SrFe <sub>2</sub> O <sub>4</sub> /diatomite (2.0 g/L)	Tetracycline	10 (in 200 mL)	Light Source: 150 W Xenon Lamp with UV light filter	150 min	92 (TOC = ~80 @ 2h)	[46]
Ce/N co-doped TiO <sub>2</sub> / NiFe <sub>2</sub> O <sub>4</sub> diatomite (0.5 g/L)	Tetracycline	20 (in 200 mL)	Light Source: 150 W Xenon Lamp with UV light filter	180 min	98.2 (TOC = ~95)	[45]
ZnFe <sub>2</sub> O <sub>4</sub> / TiO <sub>2</sub> (1.0 g/L)	Bisphenol A	10 (in 200 mL)	Light Source: 300 W Xenon Lamp pH= 7	30 min	100	[47]

#### 2.1.4. TiO<sub>2</sub>/Cu<sub>2</sub>O

Cu<sub>2</sub>O, a *p*-type semiconductor ( $E_g = 2.0\text{--}2.2\text{ eV}$ ), is also a good candidate for making heterojunctions with TiO<sub>2</sub> (*Type II Heterojunction*). Hence, the photocatalytic degradation of various CECs (TC [48], and tetrabromodiphenyl ethers [49]) using TiO<sub>2</sub>/Cu<sub>2</sub>O composite materials was reported under solar light irradiation (Table 4). Based on the findings in the mentioned studies, the photocatalytic mechanism of TiO<sub>2</sub>/Cu<sub>2</sub>O under solar light illumination involves the activation of both Cu<sub>2</sub>O and TiO<sub>2</sub> to generate  $e^-/h^+$  pairs (Figure 5). Photogenerated  $e^-$  in CB of Cu<sub>2</sub>O then can migrate to CB of TiO<sub>2</sub> and, along with photogenerated  $e^-$  in CB of TiO<sub>2</sub>, react with O<sub>2</sub> to form O<sub>2</sub><sup>•-</sup>. Simultaneously, photogenerated  $h^+$  in VB of Cu<sub>2</sub>O can be directly involved in the oxidation of adsorbed organics, while photogenerated  $h^+$  in VB of TiO<sub>2</sub> can directly oxidize adsorbed organics or react with H<sub>2</sub>O (i.e., OH<sup>-</sup>) and generate •OH. Besides, these  $h^+$  can also directly migrate to the VB of Cu<sub>2</sub>O, thus leading to effective charge separation that improves the overall photocatalytic activity of the composite [48].

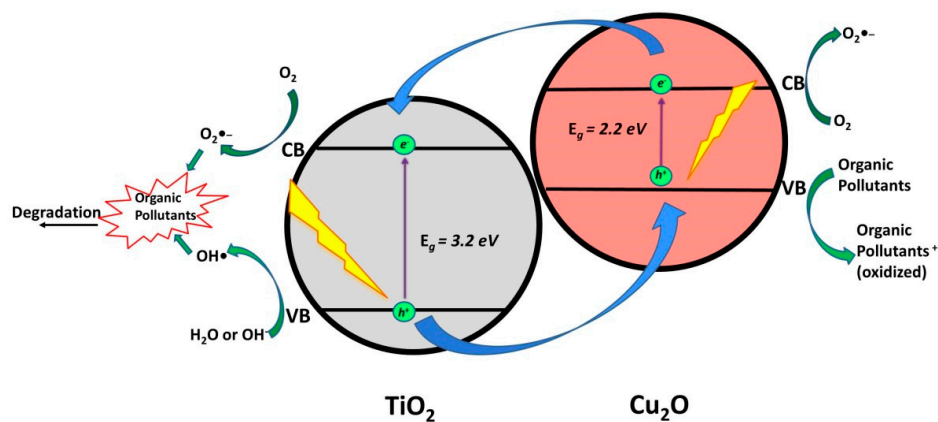


Figure 5. Photocatalytic degradation mechanism over TiO<sub>2</sub>/Cu<sub>2</sub>O composite.

#### 2.1.5. TiO<sub>2</sub>/Bi<sub>2</sub>O<sub>3</sub>

Bi<sub>2</sub>O<sub>3</sub>, a semiconductor with band gap range in the visible region (2.5–2.8 eV), is also a good candidate for making heterojunctions with TiO<sub>2</sub> (*Type II Heterojunction*). Studies including its application in photocatalytic degradation of CECs (quinalphos [50] and ofloxacin [51]) under solar light irradiation (Table 5) revealed the occurring photocatalytic mechanism. Both of the composite phases can be activated under solar irradiation generating  $e^-/h^+$  pairs (Figure 6). Accordingly, photogenerated  $h^+$  in VB of TiO<sub>2</sub> are involved in the production of •OH (through reactions with H<sub>2</sub>O, i.e., OH<sup>-</sup>) as of  $e^-/h^+$  pairs. In addition,  $h^+$  in VB of Bi<sub>2</sub>O<sub>3</sub> can be transferred to VB of TiO<sub>2</sub> that contributes to the direct oxidation of adsorbed organics or the generation of •OH [51].

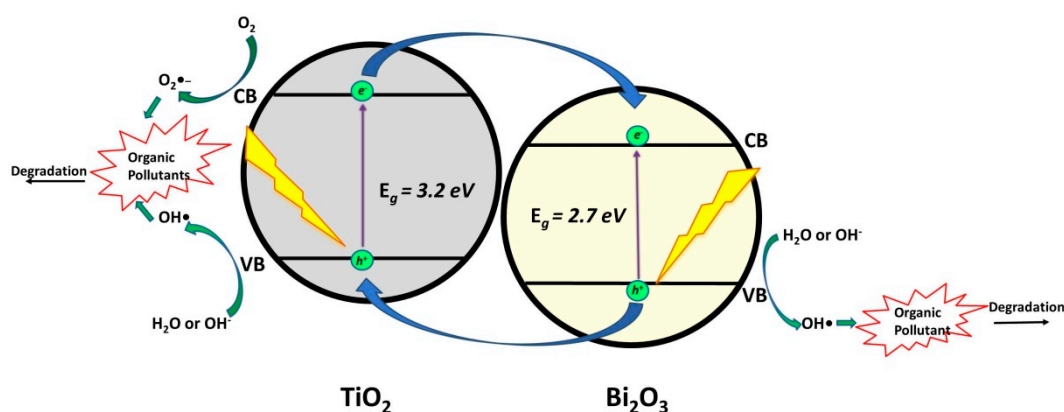


Figure 6. Photocatalytic degradation mechanism over TiO<sub>2</sub>/Bi<sub>2</sub>O<sub>3</sub> composite.

**Table 4.** Photocatalytic degradation of CEC's over TiO<sub>2</sub>/Cu<sub>2</sub>O composites.

Catalyst	Target Pollutant	Initial Concentration/ Working Volume (mg L <sup>-1</sup> )/mL)	Experimental Conditions	Reaction Time	Removal Extent (%)	Reference
Cu <sub>2</sub> O-TiO <sub>2</sub> supported palygorskite (1.0 g/L)	Tetracycline Hydrochloride	30 (in 50mL)	Light Source: 500 Xe Lamp; pH = 8.7	240 min	88.81	[48]
TiO <sub>2</sub> -Cu <sub>2</sub> O film	Tetrabromodiphenyl Ethers	5 (in 100 mL)	Light Source: 300 W Xenon Lamp; pH = natural solvent CH <sub>3</sub> OH:H <sub>2</sub> O (50:50 v/v)	150 min	90	[49]

**Table 5.** Photocatalytic degradation of CEC's over TiO<sub>2</sub>/Bi<sub>2</sub>O<sub>3</sub> composites.

Catalyst	Target Pollutant	Initial Concentration/ Working Volume (mg L <sup>-1</sup> )/mL)	Experimental Conditions	Reaction Time	Removal Extent (%)	Reference
Bi <sub>2</sub> O <sub>3</sub> -TiO <sub>2</sub> (50 mg)	Quinalphos	25 (in 50 mL)	Light Source: Visible light with 1.56μmol/m <sup>2</sup> /s; pH = 8	100 min	92	[50]
Bi <sub>2</sub> O <sub>3</sub> -TiO <sub>2</sub> (0.5 g/L)	Ofloxacin	25	Light Source: 70.3 K lux; pH = 7	120 min	92	[51]

## 2.2. Coupling of TiO<sub>2</sub> with Metal Sulfides

Cadmium sulfide (CdS), a metal sulfide semiconductor with a visible light range band gap ( $E_g = 2.1\text{--}2.4\text{ eV}$ ), has been proven to be compatible with TiO<sub>2</sub>, due to its higher position of CB than that of TiO<sub>2</sub> (*Type II Heterojunction*) (Figure 7) [25,52]. However, one should be aware that its application can lead to adverse effects due to its instability, resulting in the leaching of toxic Cd<sup>2+</sup> during treatment [53]. Although its CB and VB positions are thermodynamically favorable for photocatalytic application, CdS as a photocatalytic material faces serious problems. Next to the above-mentioned promotion of toxic effects, issues, like poor stability due to photocorrosion and limited separation efficiency of photogenerated charge carriers, do not speak in favor of CdS application [54,55]. Photocorrosion is not only related to the photogenerated  $h^+$  in semiconductor itself that oxidizes S<sup>2-</sup> and release Cd<sup>2+</sup> to the solution, but also with newly formed O<sub>2</sub>, where higher solubility in water leads to more dramatic levels of photocorrosion of CdS [54,56]. However, CdS was widely investigated in photocatalytic purposes, even in recent studies that focused on the degradation of CECs (ofloxacin, ciprofloxacin, tetracycline, and 17 $\alpha$ -ethynylestradiol), where it was used in various forms (nano-rods, nano-belts) [25,52,57,58] (Table 6). Generally, upon visible light illumination, CdS is excited and generates the  $e^-/h^+$  pair, where photogenerated  $e^-$  in CB of CdS migrates to CB of TiO<sub>2</sub> and is consumed in reactions with O<sub>2</sub> to produce O<sub>2</sub><sup>•-</sup>, while  $h^+$  remain in the VB of CdS.

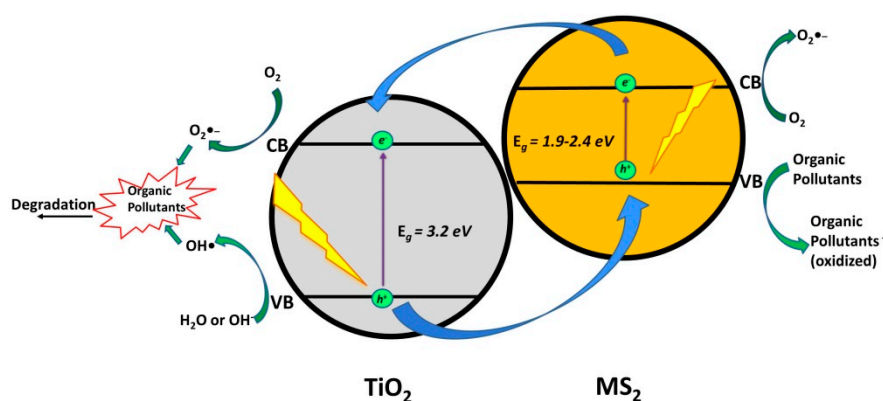


**Figure 7.** General photocatalytic degradation mechanism over TiO<sub>2</sub>/MS (M = Cd or Cu) or MS<sub>2</sub> (M = Mo and Sn) composite.

Copper sulfide (CuS), which is another metal sulfide semiconductor with narrow band gap of 2.0 eV, has also been reported to be coupled with TiO<sub>2</sub> (*Type II Heterojunction*) [59,60]. Jiang et al. [59] reported a 85.5% degradation of enrofloxacin and 27.7% mineralization of overall organic content using immobilized CuS/TiO<sub>2</sub> nanobelts (Table 6). They elucidated the mechanisms occurring in the composite upon excitation by solar irradiation. Hence, such broad wavelengths excited both composite phases (CuS and TiO<sub>2</sub>) and resulted in  $e^-/h^+$  pairs, while the transfer of charges was analogous, as in the case of the CdS/TiO<sub>2</sub> composite. Photogenerated  $e^-$  in CB ( $-0.33\text{ eV}$ ) of CuS underwent transfer to CB ( $-0.19\text{ eV}$ ) of TiO<sub>2</sub> and were consumed in reactions with O<sub>2</sub> forming O<sub>2</sub><sup>•-</sup>. Photogenerated  $h^+$  in VB of CuS remained there and present potential active sites for direct degradation of organics that were adsorbed at the CuS surface, since they cannot be involved in generation of •OH due to too high energy band positioning. On the other hand, photogenerated  $h^+$  in VB of TiO<sub>2</sub> can directly react with adsorbed organics and OH<sup>-</sup> generating •OH. Chen et al. [60], incorporated Au nanoparticles to CuS/TiO<sub>2</sub> nanobelts structure to enhance the photocatalytic degradation ability of the composite by capturing  $e^-$  and, consequently, suppressing the recombination of photogenerated charges. As a result, they obtained 96% degradation of OTC and 68% mineralization of the overall organic content within one hour under artificial sunlight illumination. Accordingly, the mechanism of such enriched CuS/TiO<sub>2</sub> composite involves, besides the above discussed mechanism, the path considering the transfer of  $e^-$  to Au, which leads to enhanced charge separation, thus delaying recombination. In such a case

scenario, photogenerated  $h^+$  would have higher probability to react either with adsorbed organics or with  $HO^-$  in order to generate  $\bullet OH$  (exclusively those in VB of  $TiO_2$ ), thus contributing to the overall system efficiency. The involvement of formed ROS into reaction mechanisms for OTC degradation was confirmed by scavenging tests using TB, AO, and BQ.

Molybdenum disulfide ( $MoS_2$ ), a two-dimensional (2D) layered metal chalcogenide with an indirect band gap of 1.1 eV and 1.9 eV direct band gap in monolayered form, with unique structure, low-cost, high thermal stability, and electrostatic integrity, is also a suitable candidate for forming heterojunction with  $TiO_2$  (*Type II Heterojunction*) [61–63]. Hence, Kumar et al. [64] reported its application in the photocatalytic degradation of paracetamol. Furthermore, Irandost et al. [61] applied the modified  $MoS_2/TiO_2$  composite (they used N,S-co-doped  $TiO_2$ ) in the photocatalytic degradation of DCF under visible LED lamp irradiation (Table 6). Hence, the synergistic effect of dopants in  $TiO_2$  promoted its visible light activity, yielding the formation of  $e^-/h^+$  pairs in both composite phases. The mechanism of charge formation and consequent transfer was similar, as described above for  $CuS/TiO_2$ , which was excited by solar irradiation. Hence, photogenerated  $e^-$  in CB of N,S-co doped  $TiO_2$  and CB of  $MoS_2$  were able to undergo reactions with  $O_2$  forming  $O_2^{\bullet-}$ , while  $h^+$  in VB of  $TiO_2$  promoted  $\bullet OH$  formation in reactions with  $HO^-$  and provide the direct oxidation of adsorbed organics, while, again,  $h^+$  in  $MoS_2$  were able to do only the latter. The importance of  $\bullet OH$  and  $h^+$  in DCF degradation was confirmed by trapping agents used in scavenging tests: TB and potassium iodide (KI), respectively.

Tin sulfide ( $SnS_2$ ), which is a metal sulfide semiconductor with band gap of 2.2 eV [65], has also been reported to be coupled with  $TiO_2$  (*Type II Heterojunction*) [66,67]. Hence, Kovačić et al. [66] reported improved the degradation of  $17\beta$ -estradiol (E2), for 51%, using  $SnS_2/TiO_2$  when comparing to the benchmark material (P25)  $TiO_2$  under solar irradiation. A similar improvement was obtained by comparing performances of the same materials in the case of DCF degradation [67] (Table 6). The reason for such improvement relies on the potential of photogenerated  $e^-$  in CB of  $SnS_2$  to migrate to CB of  $TiO_2$ , while  $h^+$  remained at the VB of  $SnS_2$ . In such case, the efficient separation of charges is achieved, thus facilitating the improved redox reactions, enabling effective degradation of adsorbed organics directly on the surface by  $h^+$ , in spite of the limited ability of such a composite to generate  $\bullet OH$ . Accordingly, the adsorption has been shown as an important step in the effectiveness of the  $SnS_2/TiO_2$  composite. Kovačić et al. [67] utilized DFT calculations to study the surface interaction of polar compounds (DCF) and non-polar compounds (memantine) at  $SnS_2/TiO_2$  composite and found that DCF was more efficiently degraded due to much higher adsorption ability in comparison to memantine, which is one of its structure feature limitations (amine functionality).

### 2.3. Coupling of $TiO_2$ with Silver- Based Semiconductors

Silver Phosphate ( $Ag_3PO_4$ ), a promising semiconductor with narrow band gap ( $E_g \geq 2.4$  eV), showed good photocatalytic performance in the degradation of organic pollutants under visible light irradiation [68,69]. Namely,  $Ag_3PO_4$  exhibits a quantum efficiency of up to 90% [68] and it can absorb wavelengths that are shorter than  $\sim 530$  nm [69]. Despite the qualities of  $Ag_3PO_4$  as a potential photocatalyst, it still suffers from limitations, such as photocorrosion, small but not negligible solubility in water ( $K_{sp} = 1.6 \times 10^{-16}$ ), and particle agglomeration upon synthesis [70]. To overcome these limitations, constructing a heterojunction between  $Ag_3PO_4$  and a compatible semiconductor has attracted attention due to the increase in charge separation and production of more ROS [71]. The positions of VB and CB in  $TiO_2$  directly match the  $Ag_3PO_4$  band positions, thus providing the compatibility to form a heterojunction.

Hence, Wang et al. [72] investigated the performance of  $TiO_2$  nanotubes/ $Ag_3PO_4$  quantum dots for the degradation of TC under visible light illumination, and reported a high removal rate within a short treatment period; 90% TC removal within 8 min (Table 7).

**Table 6.** Photocatalytic degradation of CEC's over TiO<sub>2</sub> /Metal sulfide composites.

Catalyst	Target Pollutant	Initial Concentration/ Working Volume (mg L <sup>-1</sup> )/mL)	Experimental Conditions	Reaction Time	Removal Extent (%)	Reference
CdS –TiO <sub>2</sub> (50 mg)	Tetracycline Hydrochloride	50 (in 50mL)	Light Source: 500 W Xenon Lamp with filter ( $\lambda > 400$ nm); pH = natural	480 min	87.0	[58]
Au-CdS/TiO <sub>2</sub> nanowire (20 mg)	Ciprofloxacin	20	Average solar light intensity = 100,000	60 min	99	[57]
CdS/TiO <sub>2</sub> (450 mg)	Ofloxacin	10 (in 100mL)	Light Source: 85 W Oreva bulb with 4150 lumens ( $\lambda = 450$ -650 nm); pH = natural	180 min	86	[52]
CdS nano-rod/TiO <sub>2</sub> nano-belt (0.50 g/L)	17 $\alpha$ -ethynylestradiol	3 (in 10 mL)	Light Source: 500 W Xenon Lamp with filter ( $\lambda > 420$ nm); pH = natural	120 min	92	[25]
CuS/TiO <sub>2</sub> nanobelts	Enrofloxacin	5 (in 35 mL)	Light Source: 35 W Xenon Lamp; pH = natural	120 min	85.5 (TOC = 27.7)	[59]
Au-CuS-TiO <sub>2</sub> nanobelts	Oxytetracycline	5 ( in 35 mL)	Light Source: 35 W Xenon Lamp; pH = natural	60 min	96 (TOC = 68)	[60]
MoS <sub>2</sub> /TiO <sub>2</sub> (25 mg/L)	Acetaminophen	302	Light Source: Sunlight; pH = natural	25 min	40	[64]
N,S co-doped TiO <sub>2</sub> @MoS <sub>2</sub> (0.98g/L)	Diclofenac	0.15 ( in 100 mL)	Light Source: 60 W LED lamp; pH = 5.5	150 min	98	[61]
TiO <sub>2</sub> /SnS <sub>2</sub> films	17 $\beta$ -estradiol	1.36 (in 90 mL)	Light Source: 450 W Xenon Arc Lamp	90 min	51.0	[66]
TiO <sub>2</sub> /SnS <sub>2</sub> films	Diclofenac	31.8 ( in 90mL)	Light Source: 450 W Xenon Arc Lamp; pH = 4	60 min	76.21	[67]

**Table 7.** Photocatalytic degradation of CEC's over TiO<sub>2</sub>/Silver-Based Semiconductor composites.

Catalyst	Target Pollutant	Initial Concentration/ Working Volume (mg L <sup>-1</sup> /mL)	Experimental Conditions	Reaction Time	Removal Extent (%)	Reference
Ti <sup>3+</sup> -doped TiO <sub>2</sub> nanotubes/ Ag <sub>3</sub> PO <sub>4</sub> quantum dots (0.5 g/L)	Tetracycline	10 (NA)	Light Source: 400 W Xenon Lamp; pH = natural	8 min	90	[72]
TiO <sub>2</sub> nanotube/ Ag <sub>3</sub> PO <sub>4</sub> nanoparticles (40 mg)	Ciprofloxacin	10 (in 40 mL)	Light Source: 300 W Xenon Lamp	60 min	85.3	[73]
TiO <sub>2-x</sub> / Ag <sub>3</sub> PO <sub>4</sub> (100 mg)	Bisphenol A	10 (in 100 mL)	Light Source: 500 W Xenon Lamp with filter (λ = 420 nm); pH = natural	16 min	95	[74]
Ag <sub>2</sub> O/ TiO <sub>2</sub> quantum dots (0.25 g/L)	Levofloxacin	10 (in 100 mL)	Light Source: 85 W Oreva CFL (4150 lumens) (λ = 380–700 nm) pH=4	90 min	81	[27]
Ag <sub>2</sub> O/TiO <sub>2</sub> -zeolite (50 mg)	Norfloxacin	5 (in 100 mL)	Light Source: 35 W Xenon Lamp	60 min	98.7 (TOC = 83.1)	[28]



The conventional heterojunction transfer mechanism (Figure 8a) explains that the photogenerated  $h^+$  in the composite would be promoted from the VB of  $Ag_3PO_4$  to VB of  $Ti^{3+}$ -doped  $TiO_2$  nanotubes, where can react with  $H_2O$  or  $HO^-$  forming  $\bullet OH$ . Simultaneously, photogenerated  $e^-$  from the  $Ti^{3+}$ -doped  $TiO_2$  nanotubes CB can react with  $O_2$  forming  $O_2^{\bullet-}$  or may transfer to the CB of  $Ag_3PO_4$ . However,  $O_2^{\bullet-}$  are not formed in  $Ag_3PO_4$ , due to the fact that the position of its CB is lower than the standard reduction potential of  $O_2^{\bullet-}/O_2$ . Wang et al. [72] concluded that TC was primarily degraded by  $O_2^{\bullet-}$  and photogenerated  $h^+$  based on the results of the conducted electron trapping experiments. Accordingly, they have extended the study by proposing a Z-scheme heterojunction transfer mechanism (Figure 8b). Under this mechanism,  $Ag(0)$  acts a recombination center, “collecting” photogenerated  $e^-$  from CB of  $Ag_3PO_4$ , where they undergo recombination with the photogenerated  $h^+$  from VB of  $Ti^{3+}$ -doped  $TiO_2$  nanotubes. In such case, photogenerated  $h^+$  on VB of  $Ag_3PO_4$  might participate in the direct oxidation reactions with adsorbed organics, while the photogenerated  $e^-$  in the CB of  $Ti^{3+}$ -doped  $TiO_2$  nanotubes can be involved in forming desired ROS,  $O_2^{\bullet-}$ , thus contributing to the enhanced performance of composite photocatalyst. Du et al. [73] applied analogue  $TiO_2/Ag_3PO_4$  composite employing  $TiO_2$  nanotube arrays for the degradation of ciprofloxacin (CIP) under solar irradiation and reported that 85.3% removal of CIP within 60 min. was facilitated through the above-mentioned mechanisms. Furthermore, Liu et al. [74] reported 95% degradation of BPA in 16 min. using  $TiO_{2-x}/Ag_3PO_4$  under visible light irradiation (Table 7). They reported that both composite phases,  $TiO_{2-x}$  and  $Ag_3PO_4$ , were excited and generated  $e^-/h^+$  pairs. Hence, photogenerated  $h^+$  in VB of  $TiO_{2-x}$  are promoted to VB of  $Ag_3PO_4$  and contributed to the direct oxidation of adsorbed organics, similarly as reported in the study by Wang et al. [72]. Photogenerated  $e^-$  from the CB of  $Ag_3PO_4$  are transferred to oxygen vacancies ( $V_o$ ) of  $TiO_2$  and contributed in reactions with adsorbed  $O_2$  generating  $O_2^{\bullet-}$  (Figure 9). They also investigated the role of these species in the degradation of BPA and found, based on monitoring BPA degradation pathway by LC/MS analysis, that intermediates are formed through two pathways: 1) hydroxylation, through reactions with  $O_2^{\bullet-}$  yielding BPA-*o*-catechol; and, 2) direct oxidation by  $h^+$  forming isopropenylphenol and phenol, which was further oxidized by  $h^+$  yielding hydroquinone and its dehydrated form benzoquinone.

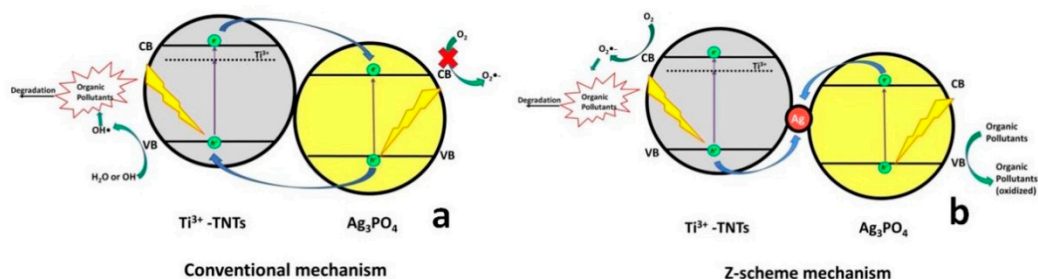


**Figure 8.** Photocatalytic mechanisms  $Ti^{3+}$ -TNTs/ $Ag_3PO_4$  (a) conventional heterojunction, and (b) Z-scheme heterojunction.

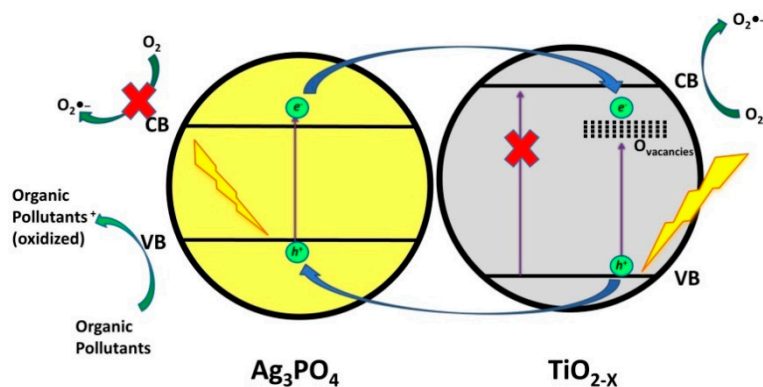


**Figure 9.** Photocatalytic reaction mechanism of  $TiO_{2-x}/Ag_3PO_4$  under visible light irradiation.

Silver oxide ( $\text{Ag}_2\text{O}$ ), a visible light active photocatalyst with band gap of 1.2 eV, is another silver-based compound with semiconducting properties. Based on the band positions (VB and CB), it represents a promising matching candidate to form heterojunctions with  $\text{TiO}_2$  (*Type III Heterojunction*). Hence, photocatalytic degradation of levofloxacin (LEV) using  $\text{Ag}_2\text{O}/\text{TiO}_2$  quantum dots is reported with the maximum of 81% LEV degradation within 90 min. of visible light irradiation [27]. Based on the proposed mechanism under visible light illumination (Figure 10), upon excitation of  $\text{Ag}_2\text{O}$ ,  $e^-/h^+$  pairs are formed, whereas  $\text{TiO}_2$  is not activated due to its wide band gap. Photogenerated  $e^-$  in the CB of  $\text{Ag}_2\text{O}$  were transferred to CB of  $\text{TiO}_2$  and involved in reactions with adsorbed  $\text{O}_2$  forming  $\text{O}_2^{\bullet-}$  that participated in LEV degradation. In addition, photogenerated  $h^+$  in VB of  $\text{Ag}_2\text{O}$  yielded the formation of  $\bullet\text{OH}$ , through reactions with  $\text{OH}^-$ , and participated in LEV degradation as well. The authors employed LC-MS analysis to elucidate LEV degradation pathway and, as such, establish the role of formed ROS. Hence, parent compound LEV underwent decarboxylation of the acetyl group; hydroxylation resulting in the formation of quinolone moieties; demethylation and the subsequent addition of hydrogen atom generating modifications at piperazine ring; while successive  $\bullet\text{OH}$  attack resulted in multi-hydroxylated intermediates. Such findings confirmed the dominant role of  $\bullet\text{OH}$  in LEV degradation.

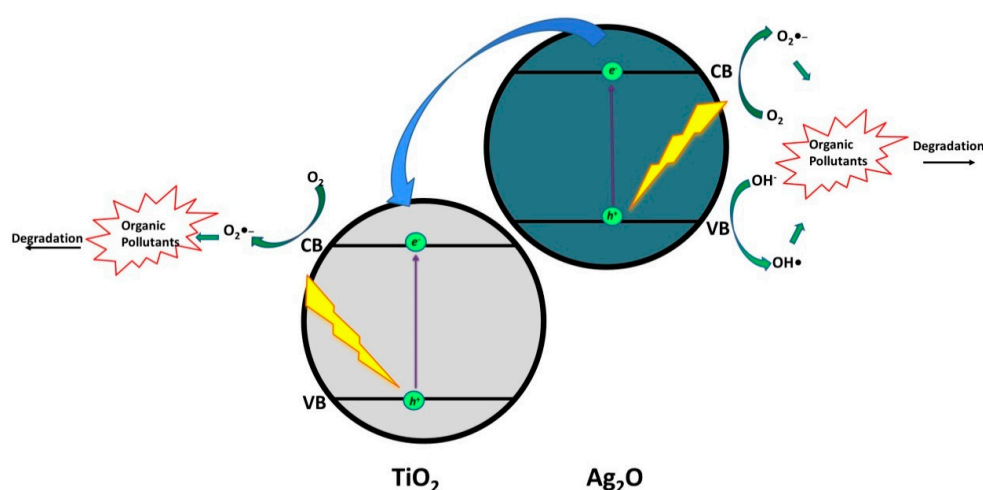


**Figure 10.** Photocatalytic degradation mechanism over  $\text{TiO}_2/\text{Ag}_2\text{O}$  composite.

In another study, Gou et al. [28] investigated the application of  $\text{Ag}_2\text{O}/\text{TiO}_2/\text{zeolite}$  composite for solar-driven degradation of norfloxacin (NOR) (Table 7). Besides high effectiveness (98.7% NOR degradation and 83.1% mineralization of organic content within 60 min. treatment), they elucidated the NOR degradation pathway, involving in the initial stage decarboxylation, defluorination or hydroxylation of parent compound (NOR), which confirmed the involvement of both formed ROS ( $\text{O}_2^{\bullet-}$  and  $\bullet\text{OH}$ ).

## 2.4. Coupling of $\text{TiO}_2$ with Graphene and Graphene-Like Materials

### 2.4.1. $\text{TiO}_2$ /Graphene Composites

Graphene is a zero bandgap semiconductor with a sheet-like structure (i.e., it is considered as a 2D monolayer material) consisting of  $\text{sp}^2$  hybridized carbon atoms with excellent thermal conductivity, optical transmittance, high mechanical strength, large surface area ( $2600 \text{ m}^2/\text{g}$ ), and appreciable charge carrier transport [75]. Under light illumination, it can achieve a reverse saturation state with high density ( $\sim 10^{13} \text{ cm}^{-2}$ ) of hot electrons above the Fermi level, which can be used as a powerful agent in redox reactions [76]. It was also found that the incorporation of graphene-based materials (i.e., graphene oxide and its reduced form; GO and rGO, respectively) with  $\text{TiO}_2$  might suppress  $e^-/h^+$  pairs recombination. As such,  $\text{TiO}_2/\text{graphene}$ -based composites were employed in the photocatalytic degradation of CECs (Table 8).

**Table 8.** Photocatalytic degradation of CEC's over TiO<sub>2</sub>/Semiconductor/graphene composites.

Catalyst	Target Pollutant	Initial Concentration/ Working Volume (mg L <sup>-1</sup> /mL)	Experimental Conditions	Reaction Time	Removal Extent (%)	Reference
TiO <sub>2</sub> / WO <sub>3</sub> /GO (2 mg)	Bisphenol A	20 ( in 50 mL)	Light Source: sunlight Ph = 7	7 h	93.2	[77]
Graphene-WO <sub>3</sub> /TiO <sub>2</sub> nanotube (photoelectrodes )	Dimethyl Phthalate	10 (in 40 mL)	Light Source: 150W Xe lamps	120 min	75.9	[78]
TiO <sub>2</sub> /ZnO/GO (0.5 g/L)	Bisphenol A	10 (in 50 mL)	Light Source: 18 UV lamps (λ =365 nm) ;Visible metal halide lamps(λ = 400–800 nm) pH = 6	120 min. (UV) 180 min. (Vis)	99.7 (UV) 94.9 (Vis)	[79]
TiO <sub>2</sub> /ZnO/GO (0.5 g/L)	Ibuprofen	10 (in 50 mL)	Light Source: 18 UV lamps (λ = 365 nm) ;Visible metal halide lamps(λ = 400–800 nm) pH = 6	120 min. (UV) 180 min. (Vis)	98.5 (UV) 79.6 (Vis)	[79]
TiO <sub>2</sub> /ZnO/GO (0.5 g/L)	Flurbiprofen	10 ( in 50 mL)	Light Source: 18 UV lamps (λ=365 nm) ;Visible metal halide lamps(λ= 400–800 nm) pH= 6	120 min. (UV) 180 min. (Vis)	98.1(UV) 82.2 (Vis)	[79]
ZnFe <sub>2</sub> O <sub>4</sub> /rGO/TiO <sub>2</sub> (0.1 g)	Fulvic Acid	20 (in 50 mL)	Light Source: 300 W (λ=420 nm); Vol H <sub>2</sub> O <sub>2</sub> = 0.8 mL, pH= 7	180 min	95.4%	[80]
TiO <sub>2</sub> /MoS <sub>2</sub> /rGO (0.5 g/L)	Bisphenol A	10 (in 50 mL)	Light Source: 20 W (λ = 254 nm);	300 min	62.4	[81]
TiO <sub>2</sub> /BiVO <sub>4</sub> /rGO	Tetracycline	10 µg/L (NA)	Light Source: 1000 W Xe Lamp (λ = 420 nm) with filter	120 min	96.2	[82]
TiO <sub>2</sub> /BiVO <sub>4</sub> /rGO	Chlorotetracycline	10 µg/L (NA)	Light Source: 1000 W Xe Lamp (λ = 420 nm) with filter	120 min	97.5	[82]
TiO <sub>2</sub> /BiVO <sub>4</sub> /rGO	Oxytetracycline	10 µg/L (NA)	Light Source: 1000 W Xe Lamp (λ = 420 nm) with filter	120 min	98.7	[82]
TiO <sub>2</sub> /BiVO <sub>4</sub> /rGO	Doxycycline	10 µg/L (NA)	Light Source: 1000 W Xe Lamp (λ = 420 nm) with filter	120 min	99.6	[82]

#### 2.4.2. TiO<sub>2</sub>/Semiconductor/Graphene Composites

As described in above sections, the coupling of TiO<sub>2</sub> with other semiconductors promotes efficient charge transfer, eventually yielding improved photocatalytic activity. However, in most cases, the recombination is still an existing issue that needs to be suppressed. Such a double effect can be obtained by combining composite concept involving two semiconductors (even “pure” TiO<sub>2</sub>, which cannot be active under visible light) with graphene-based materials. For instance, Hao et al. [77] reported 93.2% degradation of BPA in seven hours of sunlight irradiation while using the TiO<sub>2</sub>/WO<sub>3</sub>/GO composite. The mechanism occurring in such combined composite involved the excitation of both TiO<sub>2</sub> and WO<sub>3</sub> under solar light irradiation (TiO<sub>2</sub> utilized UV-A fraction), yielding the generation  $e^-/h^+$  in both semiconductors. Hence, photogenerated  $e^-$  in CB of TiO<sub>2</sub> can directly react with absorbed O<sub>2</sub>, producing O<sub>2</sub><sup>•-</sup>, or it can be transferred to CB of WO<sub>3</sub>, and then further migrate to GO enhancing charge separation. Since the amount of adsorbed O<sub>2</sub> is quite limited, the tendency of  $e^-$  to recombine with  $h^+$  is rather favored; ~90% of pairs recombine rapidly after excitation [14]. Hence, the charge separation represents an important factor in the evaluation of photocatalyst performance. Accordingly, in the case of effective separation and recombination suppression, as in the case with GO, photogenerated  $h^+$  in VB of activated composite components, e.g., of TiO<sub>2</sub> and WO<sub>3</sub> in the case of TiO<sub>2</sub>/WO<sub>3</sub>/GO, can be involved in a larger amount, either directly or indirectly (through formation of •OH) in the degradation of present organics. It should be noted that, in composites with two semiconductors, GO could also act as redox site, attracting photogenerated  $e^-$  and  $h^+$ , thus promoting improved surface migration of charges [77]. Table 8 summarizes several works regarding TiO<sub>2</sub>/semiconductor/GO composites employed for the degradation of CECs with analogous mechanism, as mentioned above.

#### 2.4.3. TiO<sub>2</sub>/g-C<sub>3</sub>N<sub>4</sub>

Graphitic carbon nitride (g-C<sub>3</sub>N<sub>4</sub>), a two-dimensional, metal-free polymeric  $\pi$ -conjugated semiconductor material, which has attracted a lot of attention [83–91] since the pioneering work of Wang et al. [92] in 2009, due to its high stability, visible light response with the bandgap of 2.7 eV and non-toxicity [93], thus representing a viable candidate to be applied in photocatalytic water treatment [80], has certainly been one of the most investigated photocatalysts inside carbon-based nanomaterials. It can be easily synthesized through the direct pyrolysis of nitrogen-rich precursors, such as melamine, cyanamide, dicyandiamide, and urea, but its practical application and principle drawback is low specific surface area and high rate of electron-hole recombination [83,94,95]. Therefore, g-C<sub>3</sub>N<sub>4</sub> modification to address shortcomings are needed, e.g., as an excellent candidate to form heterojunction with TiO<sub>2</sub> (*Type II Heterojunction*), due to their matched band positions (VB and CB). Hence, several studies employing g-C<sub>3</sub>N<sub>4</sub>/TiO<sub>2</sub> were focused on photocatalytic degradation of CECs (Table 9). For instance, Yang et al. [96] reported 88.1% degradation of CIP within 180 min. under visible light irradiation. The authors ascribed the improved photocatalytic activity to multiple effects: (i) an increase in the surface area of the composite; (ii) good dispersity of TiO<sub>2</sub> in g-C<sub>3</sub>N<sub>4</sub> enabling the intimately coupling of composite phases; and, (iii) extension of light absorption of the composite due to low band gap of g-C<sub>3</sub>N<sub>4</sub>. Trapping experiments that were conducted revealed that photogenerated  $h^+$  were the major reactive site involved in CIP degradation.

In another study, Li et al. [97] reported the 100% degradation of Acyclovir in 90 min. using g-C<sub>3</sub>N<sub>4</sub>/TiO<sub>2</sub> under visible light irradiation. However, after seven hours of continuous irradiation, any TOC removal was not noticed, implying the formation of rather recalcitrant intermediates with high resistance to degradation by ROS that formed within the studied system. Trapping experiments for formed reactive species elucidated that g-C<sub>3</sub>N<sub>4</sub>/TiO<sub>2</sub> under visible light irradiation only produced  $h^+$  and O<sub>2</sub><sup>•-</sup>, and not the most reactive •OH, explaining limited oxidation capability and none TOC removal in the case of acyclovir degradation. This significant contribution proves that the use of g-C<sub>3</sub>N<sub>4</sub>/TiO<sub>2</sub> under visible light irradiation must undergo careful laboratory tests regarding the susceptibility of targeted organics and their intermediates to degradation by  $h^+$  and O<sub>2</sub><sup>•-</sup> prior to considering real scale application [97].

Several studies also showed that the tailoring of composite morphology promotes improved photocatalytic efficiency. For instance, Yu et al. [98] prepared a mesoporous g-C<sub>3</sub>N<sub>4</sub>/TiO<sub>2</sub> that was applied to polysulfone ultrafiltration membranes for sulfamethoxazole (SMX) removal. It was found that mp-g-C<sub>3</sub>N<sub>4</sub>/TiO<sub>2</sub> exhibit 69% SMX degradation within 30 hours of sunlight irradiation. On the other hand, TiO<sub>2</sub> nanosheets with exposed facets (001) (core)-g-C<sub>3</sub>N<sub>4</sub> (shell) composite exhibit a higher degradation rate of 2.2 mg/min., which is 36% faster when compared to TiO<sub>2</sub> and g-C<sub>3</sub>N<sub>4</sub> physically-mixed composite. The improved effect is ascribed to the close interaction of TiO<sub>2</sub> and g-C<sub>3</sub>N<sub>4</sub> core-shell structure, whereas, in physically mixed composite the formed heterojunction is random and non-uniform [99].

The use of support materials, such as clays [100] and polymers [101], has been also utilized for improved adsorption capacity and the stability of g-C<sub>3</sub>N<sub>4</sub>/TiO<sub>2</sub> composites. For instance, Chen et al. [101] used g-C<sub>3</sub>N<sub>4</sub>-shielding polyester fiber (PET)/TiO<sub>2</sub> for photocatalytic degradation of sulfaquinolone and thiamethoxam. Interestingly, the composite removal efficiency for sulfaquinolone reached 97%, after 10 consequent cycles. Furthermore, the introduction of kaolinite with g-C<sub>3</sub>N<sub>4</sub>/TiO<sub>2</sub> improved the surface area and adsorption capacity of the composite, leading to 92% degradation of CIP in 240 min. of visible light irradiation [100].

An additional approach considers doping of metals and non-metals in TiO<sub>2</sub>, enhancing its light absorption capacity from UV absorption to visible light absorption. Thus, incorporating doped TiO<sub>2</sub> with g-C<sub>3</sub>N<sub>4</sub> structures has also attracted great attention for the degradation of CECs. For instance, S-Ag/TiO<sub>2</sub>@g-C<sub>3</sub>N<sub>4</sub> [102] was employed for the degradation of Triclosan (TS) and yielded 92.3% degradation of TS within 60 min. under visible light irradiation. Song et al. [103] fabricated a nanofibrous Co-TiO<sub>2</sub> coated with g-C<sub>3</sub>N<sub>4</sub>, which was applied to TC removal; the authors reported a consistent stability of composite photocatalyst during five consecutive cycles.

Besides doping, sensitization with dyes [104] and carbon dots [105] was also found to enhance the light absorption capacity of g-C<sub>3</sub>N<sub>4</sub>/TiO<sub>2</sub> composite. For example, D35 organic dye was applied next to g-C<sub>3</sub>N<sub>4</sub>/TiO<sub>2</sub> and it was found that the light absorption range was enhanced up to 675 nm [104]. On the other hand, Su et al. [105] studied the application of C dots decorated/g-C<sub>3</sub>N<sub>4</sub>/TiO<sub>2</sub> for the degradation of enrofloxacin under visible light and assigned the observed enhancement to the upconversion photoluminescence properties of C dots, which convert near-infrared light wavelength into visible light wavelength [106]. As effective solutions for improving g-C<sub>3</sub>N<sub>4</sub>/TiO<sub>2</sub> performance, the incorporation of graphene quantum dots [107] and another semiconductor (i.e., MoS<sub>2</sub> [108], WO<sub>3</sub> [109]) is also reported; such systems resulted in enhanced separation of charges and the suppression of their recombination, thus leading to improved photocatalytic activity in the degradation of CECs.

**Table 9.** Photocatalytic degradation of CEC's over TiO<sub>2</sub> /g-C<sub>3</sub>N<sub>4</sub> composites.

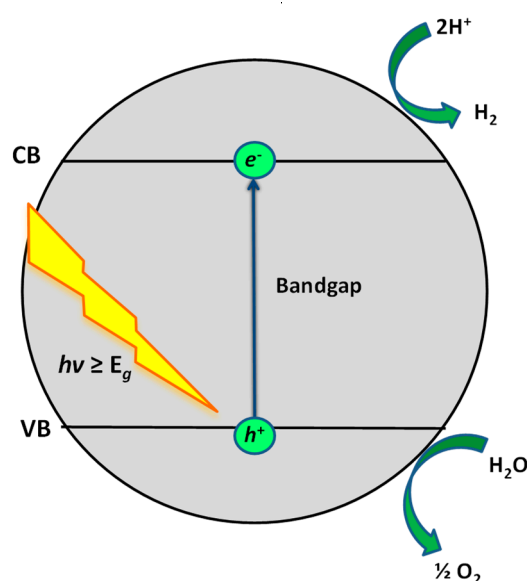
Catalyst	Target Pollutant	Initial Concentration/ Working Volume (mg L <sup>-1</sup> /mL)	Experimental Conditions	Reaction Time	Removal Extent (%)	Reference
g-C <sub>3</sub> N <sub>4</sub> /TiO <sub>2</sub> (30 mg)	Ciprofloxacin	10 (in 80 mL)	Light Source: 300 W Xe Lamp with filter ( $\lambda > 400$ nm) pH = natural	180 min	88.1	[96]
g-C <sub>3</sub> N <sub>4</sub> /TiO <sub>2</sub> (30 mg)	Acyclovir	10 (in 100 mL)	Light Source: 300 W Xe Lamp with filter ( $\lambda > 420$ nm) pH = natural	90 min	100	[97]
mpg-C <sub>3</sub> N <sub>4</sub> /TiO <sub>2</sub> (membrane)	Sulfamethoxazole	10 (in 50 mL)	Light Source: 300 W Xe Lamp pH = natural Flow rate = 13 mL/min. Membrane flux = 918 L /m <sup>2</sup> h	1800 min	69	[98]
TiO <sub>2</sub> @g-C <sub>3</sub> N <sub>4</sub> core-shell (100 mg)	Tetracycline	20 (in 100 mL)	Light Source: Xenon Lamp with full spectrum pH = natural	9 min	(2.2 mg/min.)	[99]
g-C <sub>3</sub> N <sub>4</sub> -shielding polyester/ TiO <sub>2</sub> (130 mg)	sulfaquinoxaline	$2 \times 10^{-5}$ mol/L (30 mL)	Light Source: Q-Sun Xe-1 test, pH = 7	90 min	97	[101]
g-C <sub>3</sub> N <sub>4</sub> -shielding polyester/ TiO <sub>2</sub> (130 mg)	thiamethoxam	$2 \times 10^{-5}$ mol/L (30 mL)	Light Source: Q-Sun Xe-1 test, pH = 7	180 min	~95	[101]
g-C <sub>3</sub> N <sub>4</sub> /TiO <sub>2</sub> /kaolinite (200 mg)	Ciprofloxacin	10 (in 100 mL)	Light Source: Ave. light intensity =90 mW/cm <sup>2</sup> ; Xe Lamp with filter ( $\lambda > 400$ nm), pH = natural	240 min	92	[100]
S-Ag/ TiO <sub>2</sub> @ g-C <sub>3</sub> N <sub>4</sub> (0.20 g/L)	Triclosan	10 (in 100 mL)	Light Source: 250 W Xe Lamp with filter ( $\lambda > 420$ nm), pH = 7.8	60 min	92.3 (Detoxification Efficiency= 64.3± 3.9)	[102]
Co-TiO <sub>2</sub> @g-C <sub>3</sub> N <sub>4</sub> (5 mg ; 2 × 2 cm <sup>2</sup> membranes)	Tetracycline Hydrochloride	20 (in 10 mL)	Light Source: 300 W Xe Lamp with filter ( $\lambda > 420$ nm), pH = 7	60 min.	90.8	[103]

Table 9. Cont.

Catalyst	Target Pollutant	Initial Concentration/ Working Volume ( $\text{mg L}^{-1}$ )/mL)	Experimental Conditions	Reaction Time	Removal Extent (%)	Reference
D35-TiO <sub>2</sub> /g-C <sub>3</sub> N <sub>4</sub> (0.5g/L)	Bisphenol A	10 (in 100 mL)	Light Source: 300 W Metal Halide pH = 7, Oxidant = 2mM Persulfate	15 min	100 (TOC= 50)	[104]
C dots decorated g-C <sub>3</sub> N <sub>4</sub> / TiO <sub>2</sub> (1.0 g/L)	Enrofloxacin	4 ( in 50 mL)	Light Source: 350 W Xe Lamp with filter ( $\lambda > 420$ nm) pH = natural	60 min	91.6	[105]
graphene quantum dots/ Mn-N-TiO <sub>2</sub> /g-C <sub>3</sub> N <sub>4</sub> (45 mg)	Ciprofloxacin	10 (in 80 mL)	Light Source: 300 W Xe Lamp ( $320 \leq \lambda \leq 780$ nm), pH = 7	120 min	89	[107]
graphene quantum dots/ Mn-N-TiO <sub>2</sub> /g-C <sub>3</sub> N <sub>4</sub> (45 mg)	Diethyl Phthalate	10 (in 80mL)	Light Source: 300 W Xe Lamp ( $320 \leq \lambda \leq 780$ nm), pH = 7	120 min	70.4	[107]
MoS <sub>2</sub> supported TiO <sub>2</sub> /g-C <sub>3</sub> N <sub>4</sub> (30 mg)	Atrazine	10 (in 100 mL)	Light Source: 500 W Xe Lamp ( $\lambda > 420$ nm), pH = 7	300 min	86.5	[108]
WO <sub>3</sub> -TiO <sub>2</sub> @g-C <sub>3</sub> N <sub>4</sub>	Acetylsalicylate	10 (in 100 mL)	Light Source: 500 W Metal Halide pH = natural	90 min	98	[109]
WO <sub>3</sub> -TiO <sub>2</sub> @g-C <sub>3</sub> N <sub>4</sub>	Methyl-theobromine	10 (in 100 mL)	Light Source: 500 W Metal Halide pH = natural	90 min	97	[109]

### 3. Photocatalytic Water Splitting

Photocatalytic water splitting implies a non-spontaneous process, where the light photons are used to break the water molecules assisted by a photocatalyst, which generates photoexcited charge carriers, i.e.,  $e^-/h^+$  pairs, delivering them to the solid-liquid interface, where the redox half-reactions of water oxidation and reduction are catalyzed [110,111], analogously, as described above for photocatalytic water treatment. The difference in water splitting is that photogenerated charges (i.e.,  $e^-$  and  $h^+$ ) need to react with  $H^+$  as the electron acceptor adsorbed on the photocatalyst surface or within the surrounding electrical double layer of the charged particles in order to generate  $H_2$  [112], instead of  $O_2$  generating  $O_2^{\bullet-}$ , as in photocatalytic water treatment (Figure 1). The donors are the same;  $H_2O$ , however, desired the product of such reaction is  $O_2$ . Figure 11 shows the principal mechanism of photocatalytic water splitting with the use of  $TiO_2$  semiconductor nanoparticle. The VB and CB of semiconductor or their composites have to have favorable positions in order to enable occurrence of such reactions.



**Figure 11.** The principle photocatalytic water splitting mechanism over illuminated  $TiO_2$  nanoparticle.

Generally speaking, there are two competitive processes that occur inside the photocatalyst and affect  $H_2$  evolution. Similarly as in the case of water purification, first is the charge recombination process. Such a process reduces the excited charges for  $>90\%$ , as mentioned above [14]; according to some authors, even less than 1% of photoexcited charge carriers are able to participate in the photo-redox reactions forming  $H_2$  [111]. Such a negative tendency can be improved by controlling the recombination rate [75], as also described in detail in the case of the composite materials used for water purification. The second process is the separation of photogenerated charge carriers that favor  $H_2$  evolution, also mentioned above in the case of water purification, but here with more important role [111].

The positions of CB and VB define the redox potential of photogenerated charge carriers. A CB minimum ( $CB_{min}$ ) that is smaller than 0 V vs. standard hydrogen electrode (SHE) is required for  $H_2$  generation, while the maximum of VB ( $VB_{max}$ ) has to be higher than  $O_2/H_2O$  reduction potential, by definition, in order to enable  $O_2$  evolution [112]. As mentioned above,  $H_2$  generation through this process is non-spontaneous, needing the standard Gibbs free energy change of +237 kJ/mol or 1.23 eV, and to accomplish water splitting under visible light irradiation, the bandgap of the photocatalyst should be more than 1.23 eV and less than 3.0 eV [111]. The electronic structures of diverse semiconductors fulfill the necessary conditions for the water splitting reaction, as can be seen from Figure 12.



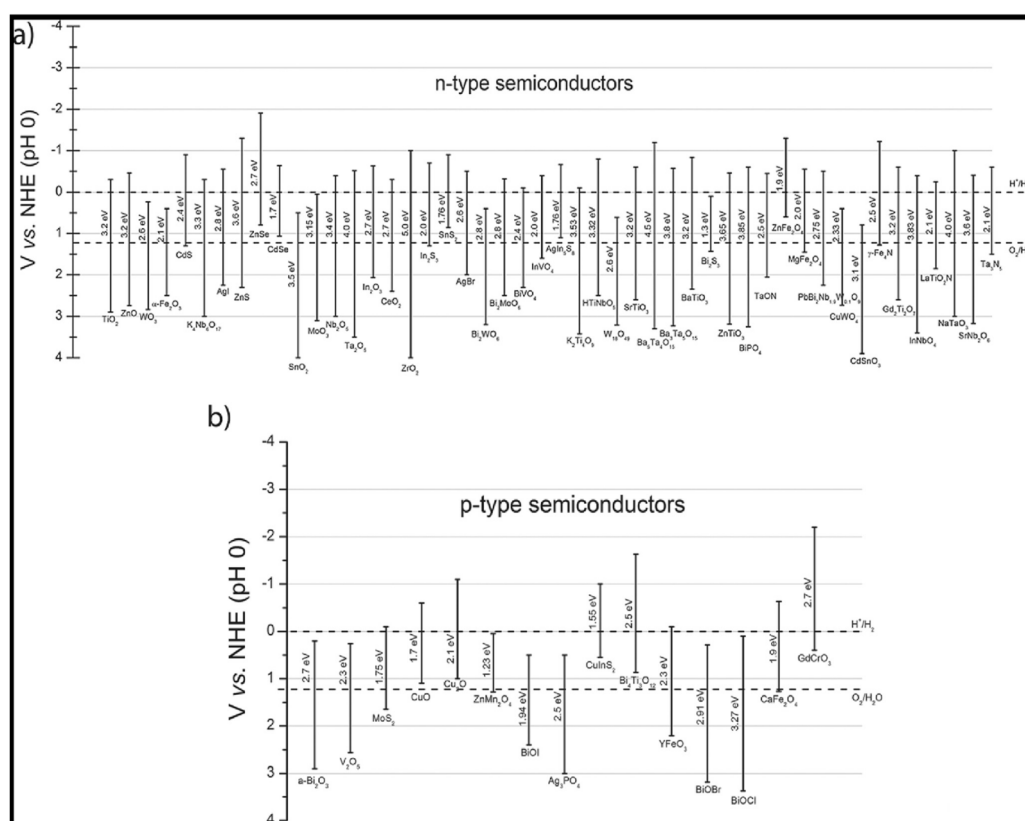


**Figure 12.** Valence band (VB) and conduction band (CB) band positions of various (a) n-type semiconductors; (b) p-type semiconductors [111].

Within the scope of this review are recent achievements in  $\text{TiO}_2$ -heterojunction systems for photocatalytic  $\text{H}_2$  generation. It is important to explain the separation mechanisms of charge carriers that occur in such hybrid materials: (i) *Schottky junctions*—photogenerated  $e^-$  migration from semiconductor to metal surface due to a higher work function of metal than those of semiconductor, thus forming a Schottky junction (Figure 13a); (ii) *Type II heterojunction* (represented in details in the case of water purification) (Figure 13b); and, (iii) *p-n Heterojunction*—supply of an additional electric field to accelerate the charge carrier transfer (Figure 13c); and, (iv) *Direct Z-scheme heterojunction*— $e^-$  in the CB of second semiconductor recombined with the photogenerated  $h^+$  in the VB of the first semiconductor, leaving the photogenerated  $e^-$  in first semiconductor and the photogenerated  $h^+$  in second semiconductor for photocatalysis (Figure 13d) [112].

The process efficiency is determined through the *Quantum yield (QY)* and *Apparent Quantum Yield (AQY)*, as described with Equations (2) and (3) [93]. The overall quantum yield is predicted to be higher than the apparent one since the number of absorbed photons is usually less than that of incident photons [111].

$$\text{QY (\%)} = \frac{\text{Number of reacted electrons}}{\text{Number of absorbed photons}} \times 100 = \frac{2 \times \text{Number of hydrogen molecules}}{\text{Number of absorbed photons}} \times 10 \quad (2)$$

$$\text{AQY (\%)} = \frac{\text{Number of reacted electrons}}{\text{Number of incident photons}} \times \quad (3)$$

$\text{H}_2$  generation can also be realized in the presence of sacrificial agents, which, in this case, serve as electron donors that accept photogenerated  $h^+$  of the VB, thus enhancing the separation of photogenerated charge carriers, which results in higher quantum efficiency [113]. Alcohols are generally used as a  $h^+$  scavenger, and the more  $\alpha$ -H atoms the alcohol has, the higher  $\text{H}_2$  production

rate is achieved due to more efficient consumption of  $h^+$  in the photoreaction. The number of  $\alpha$ -H atoms in the alcohols can serve as the reference when selecting an appropriate scavenger for photocatalytic reaction [112].

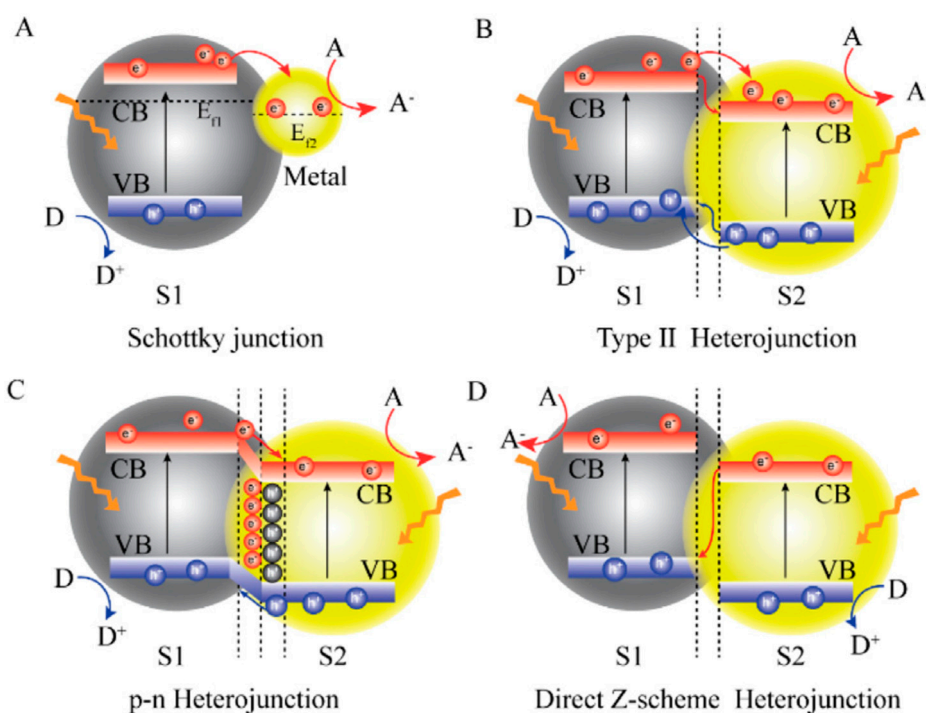


**Figure 13.** Separation mechanisms of charge carriers in hybrid materials: (A) Schottky junction; (B) Type II Heterojunction; (C) *p-n* Heterojunction; and, (D) Direct Z-scheme Heterojunction [112].

After briefly providing the basic principles to fully understand the  $H_2$  evolution through photocatalytic water splitting, following sections are more focused on the recent achievements in fabrication and the evaluation of different  $TiO_2$ -based heterojunctions with different families of materials, including carbon-based, transition metal oxides and chalcogenides, and multiple-based composites consisting of three or more semiconductor materials for  $H_2$  generation.

### 3.1. Carbon-Based/ $TiO_2$

Among a variety of materials that are selected for the preparation of  $TiO_2$ -based nanocomposites to increase their photocatalytic efficiency, nanostructured carbon materials, such as carbon nanotubes and graphene family nanomaterials (e.g., GO, rGO,  $g-C_3N_4$ ), are of particular interest [114]. The advantages, such as chemical stability, structural diversity with prominent light-absorptive, and electron transport properties, make them promising materials for use in photocatalytic  $H_2$  generation by the water splitting processes [115].

#### 3.1.1. $TiO_2/g-C_3N_4$

The advantages and limitations of  $g-C_3N_4$  are already mentioned above in the case of water treatment. The limitations referring to low light utilization efficiency and insufficient surface area can be easily broken by the preparation of 2D nanomaterials, especially  $g-C_3N_4$  nanosheets (CNNS) [84]. The self-assembly method of construction 2D/2D  $TiO_2/CNNS$  heterojunction composites achieved a hydrogen evolution rate (HER) of  $350 \mu\text{mol/h/g}$  under visible light, in comparison with the produced  $H_2$  with the use of pure  $TiO_2$  nanosheets ( $20 \mu\text{mol/h/g}$ ) and  $g-C_3N_4$  nanosheets ( $130 \mu\text{mol/h/g}$ ) [85].

Liu et al. recorded another use of CNNS [84], who synthesized partially reduced  $TiO_{2-x}$  through  $NaBH_4$  treatments with the formation of an additional mid-gap band state ( $Ti^{3+}$  and oxygen

vacancies— $O_{vs}$ ) to extend absorption edge. The implementation of novel design tactic in the form of a protective carbon layer that was coated onto  $TiO_{2-x}/CNNS$  hetero-junction photocatalyst enhanced the photocatalytic efficiency. The  $H_2$  evolution was tested under visible and simulated solar light with the use of triethanolamine (TEOA) as a sacrificial agent and Pt as a co-catalyst. In the case of visible light irradiation, the highest HER was  $417.24 \mu\text{mol/h/g}$ , while, under AM 1.5 irradiation, the obtained amount was  $1830.93 \mu\text{mol/h/g}$ . The enhanced photocatalytic activity that was ascribed to the formation of  $Ti^{3+}$  defects was also noticed with the use of  $g-C_3N_4/Ti^{3+}$ -doped  $TiO_2$  Z-scheme system that was synthesized via the polycondensation of urea with  $TiO_2$ , followed by hydrogenation treatment [86]. UV-Vis diffuse reflectance spectroscopy, X-ray photoelectron spectroscopy (XPS), and electron paramagnetic resonance (EPR) have shown that hydrogenation treatment conferred  $Ti^{3+}$  defect states that were below the  $CB_{min}$  of  $TiO_2$  and improved the visible light absorption of the composite with the obtained HER of  $1938 \mu\text{mol/h/g}$  under solar light.

Although special efforts are being made to synthesize noble-metal free nanocomposites, there is still widespread use of Pt as a co-catalyst in  $H_2$  evolution reactions. Except for the already mentioned  $TiO_{2-x}/CNNS$  photocatalyst [84],  $TiO_2/g-C_3N_4$  composites with the use of photodeposited Pt as co-catalyst reached HER of  $4128 \mu\text{mol/h/g}$  [87] and  $1041 \mu\text{mol/h/g}$  [83] under solar and visible light irradiation, respectively. Pan et al. [88] also exhibited a high HER of  $13800 \mu\text{mol/h/m}^2$  by the use of Pt as a co-catalyst with  $g-C_3N_4/TiO_2$  nanofilm. Enhanced activity is also attributed to the use of a magnetic-driven rotating frame, which was developed to enhance the mass transfer process during the photocatalytic reaction.

The charge transfer efficiency between  $TiO_2/g-C_3N_4$  composite can be enhanced by the doping of different heteroatoms, like C and K atoms. Hence, Zou et al. [89] synthesized C-doped  $TiO_2@g-C_3N_4$  core-shell hollow nanospheres with enhanced visible-light photocatalytic activity for  $H_2$  evolution of  $35.6 \mu\text{mol/h/g}$ , which was 22.7 and 10.5 times higher than that of C- $TiO_2$  and  $g-C_3N_4$ . The structure of  $TiO_2$  hollow spheres resulted in the reflection of light within the interior cavity, thus increasing the utilization of the light energy. Ma et al. [90] prepared a series of K intercalated  $g-C_3N_4$  modified  $TiO_2$  nanobelts with enhanced light absorption, transfer efficiency, and  $H_2$  evolution efficiency of  $50 \mu\text{mol/h}$ , which is 6.4 times greater than that of pristine  $g-C_3N_4$ . The use of carbon atoms in the form of carbon quantum dots (CQDs) as electron reservoirs improves the efficiency of separating the photogenerated charge carriers. CQDs present an important class of carbon materials since their discovery in 2004 by Xu et al. [116], with varying sizes in the range of 1–10 nm. They are good materials for photocatalytic applications due to features, like superiority in chemical stability and low toxicity [117]. Pan et al. synthesized the 2D carbon quantum dots modified porous  $g-C_3N_4/TiO_2$  nano-heterojunction [91] and reached  $6.497 \mu\text{mol/h/g}$  of produced  $H_2$  with the full spectrum absorption.

### 3.1.2. $TiO_2$ -G/GO/rGO

Following above-mentioned hot-electron mechanism, which can promote redox reactions, Lu et al. explored 3D graphene materials (3DG) coupled with  $TiO_2$  [76] for efficient photocatalytic  $H_2$  production under UV-visible light.  $TiO_2/3DG$  with a 5 wt.% graphene loading that was annealed at  $650^\circ\text{C}$  exhibited the highest  $H_2$  evolution rate of  $1205 \mu\text{mol/h/g}$ .

Yi et al. [118] synthesized a composite in which  $TiO_2$  nanobelts were supported by N-doped graphene (NG) coordinated with a single Co atom to replace noble metals with a cost-effective photocatalyst. Under simulated solar irradiation (Figure 14),  $e^-/h^+$  pairs are formed. The transfer of photogenerated  $e^-$  from the CB of  $TiO_2$  to Co-NG was energetically favorable since the Fermi energy level of graphene ( $-0.08\text{V}$  vs. NHE) is lower than the CB of  $TiO_2$  ( $-0.39\text{V}$  vs. NHE). NG, with a large specific surface area, acted as “freeway” for  $e^-$  transportation, delivering  $e^-$  from  $TiO_2$  to Co single-atom, where they were trapped catalyzing  $H^+$  reduction to form  $H_2$  due to lower the overpotential needed for Co-NG when comparing to that of NG. Co-NG/ $TiO_2$  showed HER of  $677.44 \mu\text{mol/h/g}$  under the illumination of AM 1.5 G simulated sunlight.

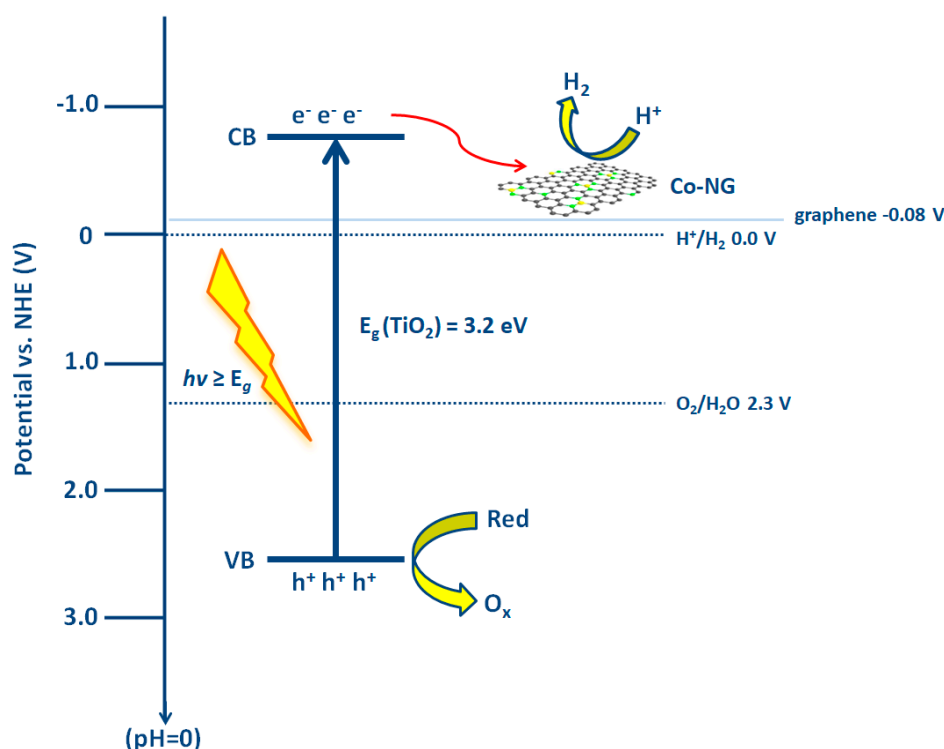


**Figure 14.** Schematic diagram of proposed photocatalytic mechanism in the CO-NG/TiO<sub>2</sub> system.

GO/TiO<sub>2</sub> nanocomposites have recently been used for H<sub>2</sub> production *via* photocatalytic water splitting under visible light through the formation of Ti-O-C bonding by unpaired  $\pi$  electron of GO with TiO<sub>2</sub> surface [114,119]. GO acts as an  $e^-$  acceptor, promoting the separation of the photogenerated  $e^-/h^+$  pairs in TiO<sub>2</sub>. These nanocomposites can be synthesized by photo assisted reduction via mixing or sonication and by sol-gel [114]. Hernández-Majalca et al. [114] enhanced the synthesis for the GO-TiO<sub>2</sub> nanocomposite using photoassisted anchoring and modifying GO oxidation method through the use of microwaves. The obtained nonporous product had a specific surface area of 45 m<sup>2</sup>/g and absorption onset of 477 nm, which made it active under visible light. Finally, the photocatalytic activity of the nanocomposite was enhanced towards the production of H<sub>2</sub>, reaching 6500 mol/g in 8 h, which was much higher amount when comparing to that obtained by TiO<sub>2</sub>-P25 (460 mol/g) at the same irradiation time.

The reduced form of GO, rGO, is a two-dimensional carbon material with the role of an electron mediator that is much superior in chemical stability and morphological diversity than GO [120]. Iwase et al. published the very first report using rGO as a  $e^-$  mediator in 2011 [121]. Since then, a number of published works were recorded for the use of rGO-based composites in photocatalytic H<sub>2</sub> production [75,122,123]. Recent achievements in the synthesis of TiO<sub>2</sub>/rGO composites for the purpose of H<sub>2</sub> generation include work from Reedy et al. [75] and Samal et al. [122]. They obtained rather high HERs while using TiO<sub>2</sub>/rGO composites under solar and visible light: 24880  $\mu\text{mol}/\text{h}/\text{g}$  and 2700  $\mu\text{mol}/\text{h}/\text{g}$  of produced H<sub>2</sub>, respectively. Ida et al. undertook further investigation on TiO<sub>2</sub>/rGO composites [123], managing to enhance the photocatalytic activity of the obtained composite by the simultaneous doping of nitrogen on TiO<sub>2</sub> and rGO. The following values for the HER are obtained: TiO<sub>2</sub> (1585  $\mu\text{mol}/\text{h}/\text{g}$ ) < N-TiO<sub>2</sub> (6179  $\mu\text{mol}/\text{h}/\text{g}$ ) < TiO<sub>2</sub>/RGO (12244  $\mu\text{mol}/\text{h}/\text{g}$ ) < N-TiO<sub>2</sub>/N-RGO (15,028  $\mu\text{mol}/\text{h}/\text{g}$ ).

### 3.1.3. TiO<sub>2</sub>/CNT

Recently, TiO<sub>2</sub>/carbon nanotubes (CNT) have been of great interest due to their high-quality active sites, large specific surface area, and retention of charge recombination, where CNTs can act as a  $p$ -type

semiconductor, having a role as a powerful electron sink [119]. The coupling of CNT with TiO<sub>2</sub> forms an advanced nanocomposite with enhanced quantum efficiency that forms heterojunction acting as an impurity by forming Ti-O-C or Ti-C defects that enable visible light absorption and, consequently, the creation of  $e^-/h^+$  pairs and hindering  $e^-/h^+$  recombination [124]. CNTs, such as single-wall carbon nanotubes (SWCNTs) and multiwall carbon nanotubes (MWCNTs), have attracted much interest due to their unique chemical, electrical, and optical properties [125]. Olowoyo et al. [124] prepared a series of TiO<sub>2</sub> nanoparticles that were modified with MWCNTs by a combined sonochemical-hydrothermal method. The synthesized photocatalysts were examined for water splitting under batch conditions at different pH ranges. The highest rate of H<sub>2</sub> yield, amounting 69.41  $\mu\text{mol/h/g}$ , was obtained using 2 wt.% CNT-TiO<sub>2</sub> under visible light at pH 2. Hence, the acidic medium improved the photocatalytic feasibility of the system due to a higher concentration of H<sup>+</sup> ions, serving as the reactants, thus increasing the reaction rate.

Bellamkonda et al. [126] used a different approach in synthesizing CNT-G-TiO<sub>2</sub> composites and prepared nanocomposites via the solution-based method, in which nanocrystalline anatase TiO<sub>2</sub> was grown onto graphene nanosheets and carbon nanotubes. Spectroscopic and photocatalytic studies revealed that graphene acts as an electron reservoir, while the role of CNTs is to prevent the restacking of graphene nanosheets and provide additional electron transport channels, thereby suppressing the recombination rate of  $e^-/h^+$  pairs in the obtained composite. The combination of all these factors resulted in increasing the HER from 19000  $\mu\text{mol/h/g}$  (obtained by anatase TiO<sub>2</sub>) to 22000  $\mu\text{mol/h/g}$  (obtained by G-TiO<sub>2</sub>), and finally to 29000  $\mu\text{mol/h/g}$  (obtained by CNT-G-TiO<sub>2</sub>), which is 8-fold higher than obtained by the commercial TiO<sub>2</sub> (Degussa P25).

The photocatalytic performance of TiO<sub>2</sub> under visible light can be promoted by coupling both MWCNTs and SWCNTs, as presented by Umer et al. [125]. Such an effect occurs due to their dual natural behavior, such as reducing rapid recombination of  $e^-/h^+$  pairs and providing support in harvesting visible light. The maximum H<sub>2</sub> evolution rate of 5486  $\mu\text{mol/h/g}$  was achieved over MWCNT/TiO<sub>2</sub>/SWCNT, which is 1.24- and 1.42-fold higher than using single CTN-TiO<sub>2</sub> composites (SWCNT/TiO<sub>2</sub> and MWCNT/TiO<sub>2</sub>, respectively).

### 3.2. Transition-Metal Oxides/TiO<sub>2</sub>

Excellent chemical stability has opened the possibility of the application of transition metal oxides (TMO) in the field of clean energy production. The above displayed Figure 12 contains main TMOs, like *p*-type (CuO, V<sub>2</sub>O<sub>5</sub>) and *n*-type (TiO<sub>2</sub>, WO<sub>3</sub>, MoO<sub>3</sub>, ZnO, Fe<sub>2</sub>O<sub>3</sub>) semiconductors that are used in photocatalytic H<sub>2</sub> production with pertaining VB and CB energy levels. Visible-light driven TMOs with narrow band gaps are highly desired. The most used materials within this group, such as CuO, Fe<sub>2</sub>O<sub>3</sub>, and WO<sub>3</sub>, have the bandgap energies that allow for them to be active in the visible light region, but the low energy levels of CB position disable them from consuming photoinduced electrons in reactions yielding H<sub>2</sub>. By changing the morphologies of desired components and co-doping with different elements, their CB and VB edges can be shifted toward a H<sub>2</sub> reduction and O<sub>2</sub> oxidation potential [127].

Some TMOs, specifically WO<sub>3</sub>, have been loaded with a different co-catalyst, like Rh, to effectively produce H<sub>2</sub> from water, to control the desired morphology in the form of nanorods, nanotubes, and nanowires. Camposeco et al. [128] focused on the use of Rh-WO<sub>3</sub> photocatalyst that was supported on TiO<sub>2</sub> nanotubes (Rh-WO<sub>3</sub>/NT) for H<sub>2</sub> production via the water splitting process. WO<sub>3</sub> alone cannot take part in H<sub>2</sub> production since the CB energy level of WO<sub>3</sub> is lower than H<sub>2</sub> reduction potential. However, by loading with Rh nanoparticles, the enhancement in H<sub>2</sub> production was noticed. An analysis of energy band levels for the VB and CB that were determined by UV-Vis results and XPS spectra showed that the presence of WO<sub>3</sub> and Rh in the titanate nanotubes simultaneously shift the VB<sub>max</sub> and CB<sub>min</sub>, thus reducing the bandgap of titanate nanotubes. 0.5 wt.% Rh- 3 wt.% WO<sub>3</sub>/NT nanocomposite under visible light irradiation yielded HER of 87  $\mu\text{mol/h}$ , while 3 wt.% WO<sub>3</sub>/NT showed much lower effectiveness (only 13  $\mu\text{mol/h}$ ).

In another work, Ren et al. [129] constructed cooperative Schottky and *p-n* (SPN) heterojunction by forming a NiO/Ni/TiO<sub>2</sub> heterostructure that showed a narrower band gap, higher photocurrent density,

and ability to absorb light in the visible region. High HER is obtained for the observed composite, amounting 4653  $\mu\text{mol/h/g}$ , which is approx. 2.3 times higher than obtained with NiO/TiO<sub>2</sub> with a *p-n* junction (2059  $\mu\text{mol/h/g}$ ), under visible light irradiation and by the use of Pt as a co-catalyst.

A representative example of TMOs is also hematite (Fe<sub>2</sub>O<sub>3</sub>), already referred above to as promising visible light active photocatalyst for water treatment. The coupling of Fe<sub>2</sub>O<sub>3</sub> with TiO<sub>2</sub> efficiently inhibits the recombination of photogenerated charge carriers and enhances the absorption of solar light [130]. By the use of thermal decomposition of FeCl<sub>3</sub> and TiCl<sub>4</sub> as precursors, Bhagya et al. [113] synthesized the Fe<sub>2</sub>O<sub>3</sub>-TiO<sub>2</sub> composite and investigated its photocatalytic activity for H<sub>2</sub> production under the influence of different proton sources. Besides focusing on the use of TMOs for improving photocatalytic efficiency, this work also highlights the influence of different sacrificial agents as electron donors that consume photogenerated  $h^+$ , yielding H<sub>2</sub> production. Under simulated solar irradiation, a very high H<sub>2</sub> rate of 880  $\mu\text{mol/h}$ , with an apparent quantum efficiency of 19.39%, is achieved while using Fe<sub>2</sub>O<sub>3</sub>-TiO<sub>2</sub> and diethylamine hydrogen chloride (DAH), which is much higher than that obtained in the case without DAH (323  $\mu\text{mol/h}$ ). Madhumitha et al. [130] also explored the influence of different sacrificial reagents on H<sub>2</sub> production under a visible light source. With the optimization of parameters, i.e., catalyst dosage, flow rate, incident light irradiation, and type of sacrificial agent, they achieved the maximum of HER, amounting 2700  $\mu\text{mol/h}$ . The increase in photoactivity was attributed to the effective charge transfer from TiO<sub>2</sub> to Fe<sub>2</sub>O<sub>3</sub> and the use of EDTA, which suppressed the recombination of photogenerated charge carriers.

Easy preparation, environmental friendliness, and good re-utilization enable the wide use of ZnO/TiO<sub>2</sub>-based composites. Xie et al. [131] achieved high rates of H<sub>2</sub> evolution while using ZnO/TiO<sub>2</sub> composites with Pt as a co-catalyst. Under visible light irradiation, 2150  $\mu\text{mol/h/g}$  of H<sub>2</sub> is achieved. Additionally, high carrier mobility can be achieved by the use of ZnO in the form of quantum dots (QDs), which presents ideal heavy-metal free “green” modification of TiO<sub>2</sub> composites. Chen et al. obtained the fabrication of ZnO QDs decorated TiO<sub>2</sub> nanowires via a facile calcination method [132]. They used the obtained composite under solar irradiation next to Pt as a co-catalyst and achieved HER of 313.5  $\mu\text{mol/h}$ .

The use of TMO QDs is also recorded in the work of Liu et al. [133], who decorated two-dimensional TiO<sub>2</sub> nanobelts with zero-dimensional Co<sub>3</sub>O<sub>4</sub> quantum dots. When compared with bulk materials, 0D Co<sub>3</sub>O<sub>4</sub> QDs have attracted considerable attention due to their small size (<10 nm), providing a large specific surface area with more active sites and shorter charges transport paths. Due to the decoration of Co<sub>3</sub>O<sub>4</sub> QDs, the bandgap of the obtained composite was also narrowed, and in application next to Pt as co-catalyst, they obtained a rather high HER of 1735.1  $\mu\text{mol/h/g}$ . In comparison, Zhang et al. [134], with the use of bulk *p*-Co<sub>3</sub>O<sub>4</sub>/*n*-TiO<sub>2</sub>, achieved a smaller HER of 8.16  $\mu\text{mol/h/g}$ .

Among the TMOs that appear as promising candidates for coupling with TiO<sub>2</sub>, CuO is one of such, especially due to its narrow bandgap (1.4–1.6 eV) and the promotion of effective charge separation [5,135], as already reported as promising water treatment photocatalyst. Hasan et al. [5] conducted solar H<sub>2</sub> production using a TiO<sub>2</sub>/CuO nanofiber composite that was synthesized by electrospinning technique. Fabricated nanofibers were annealed in different atmospheres to determine the crystalline phase and photocatalytic performance. For the nanofibers that were crystallized in the anatase phase, EPR and XRD analysis referred to the substitution of some Ti<sup>4+</sup> ions by Cu<sup>2+</sup> ions, leading to the formation of some defects below the CB of TiO<sub>2</sub>, which led to a narrow band gap, yielding enhanced HER in the amount of 2715  $\mu\text{mol/h/g}$ . For comparison, without annealing in a different atmosphere, Wang et al. [135] only achieved 47  $\mu\text{mol/h/g}$  of produced H<sub>2</sub> while using the TiO<sub>2</sub>/CuO composite that was irradiated by solar light. Other oxidation states of Cu inside the oxides are investigated for coupling with TiO<sub>2</sub>, such as Cu<sub>2</sub>O [136]. With all of the benefits, such as environmental compatibility, high visible light activity and earth abundance, wider applications of Cu<sub>2</sub>O in water splitting are still limiting, since the redox potential of monovalent copper lies within its band gap, thus photogenerated charge carriers thermodynamically prefer the transformation of Cu<sub>2</sub>O into CuO and Cu, rather than to be used in redox reactions with water constituents forming H<sub>2</sub> [136]. Wei et al. [136] stabilized the Cu<sub>2</sub>O by modulating the defects in faceted Cu<sub>2</sub>O/TiO<sub>2</sub> heterostructures to suppress this disproportionation process. Hence, Cu<sub>2</sub>O was

arranged onto 101-faceted TiO<sub>2</sub> and it was found that oxygen vacancies in {101}-faceted TiO<sub>2</sub> can create a unique channel for Z-scheme charge transfer in Cu<sub>2</sub>O/TiO<sub>2</sub> heterostructures. Composite that was obtained by such an approach showed the maximum HER of 32600 μmol/h/g, with a quantum efficiency of 53.5% at an irradiation wavelength of 350 nm.

### 3.3. Transition Metal Chalcogenides-TiO<sub>2</sub>

As already mentioned, various techniques have been applied to modify the TiO<sub>2</sub> photocatalysts with a purpose of wider application in the field of solar-driven H<sub>2</sub> production through water splitting. Sensitization with narrow bandgap semiconductors was found to be an effective method for enhancing all of the deficiencies that occur during the sole use of TiO<sub>2</sub>. Regarding an appropriate band gaps, another group of semiconductors with great application potential in photocatalytic H<sub>2</sub> generation are transition metal chalcogenides. Recently, CdS is one of the most studied materials [54,55,137–140]; however, the toxic effects due to potential leaching of Cd<sup>2+</sup> have to be strongly considered, followed by others (MoS<sub>2</sub>, ZnS, ZnSe, CdSe) indicated in Figure 12, as mentioned in part related to water treatment [127].

#### 3.3.1. TiO<sub>2</sub>/CdS

CdS is the most important chalcogenides semiconductor as a hydrogen production catalyst due to its narrow bandgap (2.4 eV), which enables its visible light response [56]. Its drawbacks described above in Section 2.2. can be alleviated; susceptibility to photocorrosion can be suppressed by the use of sacrificial agents (sodium sulfite/sulfide) that effectively consume photogenerated *h*<sup>+</sup>, while the limited separation efficiency of photogenerated charge carriers can be solved either by using CdS in the form of QDs due to a shorter transportation path or by incorporating CdS onto support materials, such as TiO<sub>2</sub> [55,56].

Rao et al. [137] synthesized CdS/TiO<sub>2</sub> core/shell nanorods with tunable shell thickness to minimize charge carriers recombination and limit photocorrosion. The investigation of photocatalytic activity performed under UV-vis light irradiation confirmed that optimized concentration of sacrificial agents (0.3 M Na<sub>2</sub>S and Na<sub>2</sub>SO<sub>4</sub> aqueous solution), shell thickness of 6.3 nm, and solution pH of 8.0 enhance the H<sub>2</sub> production rate of 5791 mL/h/g. Du et al. [138], who fabricated pyramid-like CdS nanoparticles that were grown on porous TiO<sub>2</sub>, obtained the same type of composite, but with the different morphology. Under UV-vis irradiation and without noble-metal co-catalysts, 5 mol% CdS-TiO<sub>2</sub> achieved an H<sub>2</sub> production rate of 1048.7 μmol/h/g, which is almost six times and 1.5 times higher than that of pure TiO<sub>2</sub> and CdS, respectively. Table 10 provides further examples of TiO<sub>2</sub>/CdS-based composites with their respective photocatalytic activities for H<sub>2</sub> production.

**Table 10.** The photocatalytic performance of H<sub>2</sub> generation in some related TiO<sub>2</sub>/CdS-based nanocomposites.

Photocatalyst	Light Source	HER	Reference
CdS/Pt/TiO <sub>2</sub> film	300 W Xe lamp	3.074 μmol/h/g	[54]
CdS/Pt/TiO <sub>2</sub> nanosheets	350 W Xe arc lamp	265 μmol/h	[141]
CdS/Pt/TiO <sub>2</sub> nanotubes	300 W Xe lamp	402 μmol/h	[142]
CdS/TiO <sub>2</sub> nanotubes	350 W Xe lamp	2585 μL/h/g	[143]
CdS-Ti-MCM-48-21-25	300 W Xe lamp	2726 μmol/h	[139]

#### 3.3.2. TiO<sub>2</sub>/CuS

CuS has emerged as an alternative co-catalyst for H<sub>2</sub> production, which is abundant, cheap, and nonhazardous. With its VB and CB at positions of −1.56 eV vs. NHE, and −0.09 eV, CuS shows low reflectance in the visible and relatively high reflectance in the near-infrared region, which makes it a good candidate for solar energy absorption [144]. Chandra et al. [144] investigated the photocatalytic activity for H<sub>2</sub> generation of synthesized CuS/TiO<sub>2</sub> (CT) heterostructured nanocomposite under UV-vis and only visible light. Under irradiation, the highest HER of 12362 μmol/h/g was achieved while

using 0.4 mol.% CuS/TiO<sub>2</sub>, while only 155 μmol/h/g of H<sub>2</sub> was produced under visible light and comparable conditions.

In comparison, Dang et al. [145] produced a series of Cu<sub>x</sub>S (x = 1 or 2) co-modified TiO<sub>2</sub> nanocomposites while using a one-step precipitation approach. The EDS, XPS, and XRF results confirmed the existence of three different phases: CuS, Cu<sub>2</sub>S, and TiO<sub>2</sub>. The results have shown that CuS and Cu<sub>2</sub>S dual co-catalysts under simulated solar light exhibited high H<sub>2</sub> production of 5620 μmol/h/g, which is about 58 times higher than that of the unloaded TiO<sub>2</sub>. The enhancement in H<sub>2</sub> production can be contributed to the co-deposition of CuS and Cu<sub>2</sub>S onto the TiO<sub>2</sub> nanoparticle surface that efficiently extended visible light absorption and facilitated the separation of charge carriers. The Cu<sub>x</sub>S/TiO<sub>2</sub> composite showed high stability; after three consecutive cycles the photocatalytic efficiency for H<sub>2</sub> production decreased for only 11.7%.

### 3.3.3. TiO<sub>2</sub>/MoS<sub>2</sub>

MoS<sub>2</sub> represents two-dimensional transition metal dichalcogenide (TMD) that can be prepared into ultrathin-layered structures and, thus, participates in the H<sub>2</sub> evolution reaction as an effective non-noble metal alternative [117,146]. Without the use of any sacrificial agent and co-catalyst, Huang et al. [146] observed photocatalytic H<sub>2</sub> generation while using MoS<sub>2</sub> quantum dots@TiO<sub>2</sub> nanotube arrays nanocomposite in pure water under visible light. The photocatalytic activity was influenced by the amount of MoS<sub>2</sub> QDs coated on TiO<sub>2</sub> NTAs. Hence, the maximum of 53.9 μmol/cm<sup>2</sup>/h of H<sub>2</sub> was produced, which was ascribed to the decreased bandgap and the surface plasmonic properties of the obtained composite promoting charge carrier separation and the absorption capacity to visible light. Du et al. [63] grew *in situ* two transition metal chalcogenides—MoS<sub>2</sub> and CdS—on porous TiO<sub>2</sub> by using the sol-gel method, followed by the calcination and hydrothermal method. Under visible light irradiation and without the use of noble metals as the co-catalyst, 3% MoS<sub>2</sub>-CdS-TiO<sub>2</sub> produced 4146 μmol/h/g of H<sub>2</sub>. In this ternary composite (Figure 15), the porous structure of TiO<sub>2</sub> accepts generated e<sup>-</sup> from CdS and provides surface area for H<sub>2</sub> production, while MoS<sub>2</sub>, as a conductive medium, enabled the transfer of e<sup>-</sup> between CB of CdS and TiO<sub>2</sub>, simultaneously inhibiting the photocorrosion of CdS as h<sup>+</sup> collector.

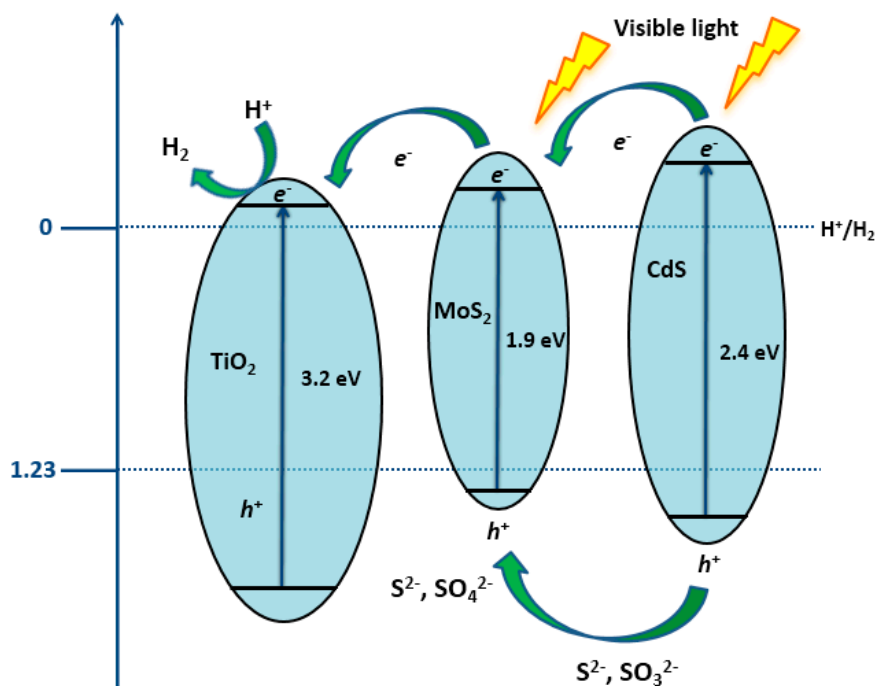


Figure 15. The proposed photocatalytic mechanism in MoS<sub>2</sub>-CdS-TiO<sub>2</sub> photocatalyst.



### 3.4. Multiple TiO<sub>2</sub>-Based Composites

This section is dedicated to multiple ternary and quaternary TiO<sub>2</sub>-based composites. Recently, significant emphasis was laid on the formation of Z-scheme structured photocatalysts. In such materials, redox reactions occur in each semiconductor, allowing for the combination of a semiconductor with strong reduction power with another semiconductor with strong oxidation power [93].

All of the solid Z-scheme heterojunctions are usually composed of two photocatalysts and an electron mediator, which enable efficient H<sub>2</sub> production through the synergistic action between two isolated photosystems and electron mediator cleverly arranged in a nano-platform [147]. Reversible redox couples (e.g., IO<sub>3</sub><sup>-</sup>/I<sup>-</sup>, Fe<sup>3+</sup>/Fe<sup>2+</sup>) are usually applied as electron mediators in the Z-scheme system. Solid electron mediators are more suitable for the application. Noble metals (Au, Ag) and carbon-based materials (MWCNT, rGO, CQDs) are commonly used as solid electron mediators for photocatalytic H<sub>2</sub> generation [148].

Ng et al. [147], who synthesized Zn<sub>0.5</sub>Cd<sub>0.5</sub>S-MWCNT-TiO<sub>2</sub> ternary nanocomposite, where MWCNT acted as an electron mediator, fabricated a solid Z-scheme system. The obtained material efficiently suppressed charge recombination and promoted water reduction, achieving HER of 21.9 μmol/h. Furthermore, Liu et al. [149] have used carbon quantum dots (QDs) as an electron mediator between TiO<sub>2</sub> and Zn<sub>0.5</sub>Cd<sub>0.5</sub>S film and achieved 38740 μmol/h/m<sup>2</sup> of produced H<sub>2</sub> under solar light. Lv et al. investigated the use of rGO as an electron mediator [120], synthesizing sandwich-like TiO<sub>2</sub>/rGO/LaFeO<sub>3</sub> ternary heterostructure, which, under solar light, obtained HER of 893 μmol/h/g, which is almost 3.2, 14.4, and 11.4 times superior to the direct Z-scheme components TiO<sub>2</sub>/LaFeO<sub>3</sub> composite, pure TiO<sub>2</sub>, and LaFeO<sub>3</sub>, respectively. The photocatalytic mechanism of H<sub>2</sub> production is the same for all three above mentioned solid electron mediators: MWCNT, rGO, and CQDs (Figure 16). Upon excitation by light, e<sup>-</sup>/h<sup>+</sup> are formed in Z-scheme semiconducting components, depending on the ability of each component to absorb emitted light. Hence, photogenerated e<sup>-</sup> from semiconductor I can be easily recombined with h<sup>+</sup> from semiconductor II through the electron mediator, leaving more oxidative holes and reductive electrons to participate in the redox reactions in the corresponding active sites [148].

In Z-type heterojunction, noble metals can also perform the role of electron mediators. Zou et al. performed the construction of g-C<sub>3</sub>N<sub>4</sub>/Au/C-TiO<sub>2</sub> hollow spheres with Au nanoparticles (NPs) as the electron mediator [150]. The as-prepared composite showed high HER of 129 μmol/h/g under visible light, which can be attributed to the efficient charge separation in the constructed Z-scheme system, the broadened visible-light response range, owing to the surface plasmon resonance (SPR) effects on Au nanoparticles, and the hollow structure of C-TiO<sub>2</sub> that gives photocatalyst unique properties of low density and high light-harvesting efficiency. In another work presented by Yang et al. [151], Au NPs were applied as a solid electron mediator in the ternary urchin-like ZnIn<sub>2</sub>S<sub>4</sub>-Au-TiO<sub>2</sub> nanocomposite, which, at an optimal ratio of 24 wt.% Au NPs and 60 wt.% ZnIn<sub>2</sub>S<sub>4</sub>, achieved HER of 186.3 μmol/h/g under solar light irradiation.

Table 11 lists other multiple composites, except ones with the Z-scheme heterojunction that are already mentioned, as well as reaction conditions in the photocatalytic system and the obtained hydrogen evolution rates.

**Table 11.** Multiple TiO<sub>2</sub>-based composites for the use in photocatalytic hydrogen generation.

Photocatalyst	Reaction Conditions	HER	Reference
CdSQDs/WC/TiO <sub>2</sub>	Photocatalyst dispersed in 20 vol.% lactic acid as an electron donor under visible light.	624.9 μmol/h/	[55]
ZnO/ZnCr <sub>2</sub> O <sub>4</sub> @TiO <sub>2</sub> -NTA	Photocatalyst dispersed in aqueous methanol solution under simulated solar light.	1680 μmol/cm <sup>2</sup>	[152]
F-TiO <sub>2</sub> /CdSe-DETA	Photocatalyst was dispersed in a mixed solution of Na <sub>2</sub> S and Na <sub>2</sub> SO <sub>3</sub> as a sacrificial agents under visible light with the use of Pt as a cocatalyst.	12381 μmol/h/g	[153]
g-C <sub>3</sub> N <sub>4</sub> /TiO <sub>2</sub> /RGO	5 mg of the g-C <sub>3</sub> N <sub>4</sub> -TiO <sub>2</sub> /RGO nano-composite was dispersed in 50 mL glycerol-water solution under UV-vis light.	19610 μmol/h/g	[13]
CDS/CNF/Pt-TiO <sub>2</sub>	Photocatalyst was dispersed in a mixed solution of Na <sub>2</sub> S and Na <sub>2</sub> SO <sub>3</sub> as a sacrificial agents under visible light.	16.34 μmol for 3 h	[154]
F-TiO <sub>2</sub> /CdS-DETA, Pt as a cocatalyst	50 mg of the photocatalyst was dispersed in 100 mL of mixed aqueous solution containing 0.35 mg/L Na <sub>2</sub> S and 0.25 mg/L Na <sub>2</sub> SO <sub>3</sub> with the use of Pt as a cocatalyst.	5342.86 μmol/h/g	[155]
CdS@TiO <sub>2</sub> @Au	20 mg of the photocatalyst was dispersed in 40 ml of aqueous solution containing 0.1 M Na <sub>2</sub> S and 0.1 M Na <sub>2</sub> SO <sub>3</sub> as the sacrificial agents under visible light.	1720 μmol/h/g	[156]
TiO <sub>2</sub> -Au-CdS	0.1 g of the sample was immersed in an aqueous solution containing 0.1 M Na <sub>2</sub> S and 0.1 M Na <sub>2</sub> SO <sub>3</sub> as the sacrificial agents under visible light.	1810 μmol/h/g	[157]
N-TiO <sub>2</sub> /g-C <sub>3</sub> N <sub>4</sub> @Ni <sub>x</sub> P	50 mg photocatalyst was suspended in a 100 mL solution containing 10 vol.% triethanolamine (TEOA) under 300 W Xe lamp irradiation.	5438 μmol/h/g	[158]
TiO <sub>2</sub> /CdS/CNT	0.1 g of photocatalyst was dispersed in solution containing 70 mL of distilled water or seawater and 30 mL of sacrificial agent. The photocatalyst were irradiated using three visible-light sunlamps of each 100 W and UV lamp of 8 W.	3502 μmol/h from pure water and 1373 μmol/h from seawater	[159]
WS <sub>2</sub> /C-TiO <sub>2</sub> /g-C <sub>3</sub> N <sub>4</sub>	50 mg of photocatalyst was added in to 80 mL TEOA aqueous solution with the use of Pt as a cocatalyst.	17726 for DI water and 29978 μmol/g for seawater	[148]
TiO <sub>2</sub> /La <sub>2</sub> O <sub>2</sub> CO <sub>3</sub> /rGO	0.05 g of powder catalyst was dispersed in 80 MI ethylene-glycol water (5/95, v/v) solution under UV-vis light.	583 μmol/h	[160]
TiO <sub>2</sub> -Cu@C	Photocatalyst was dispersed in methanol aqueous solution under UV-vis light.	3911 μmol/g/h	[161]

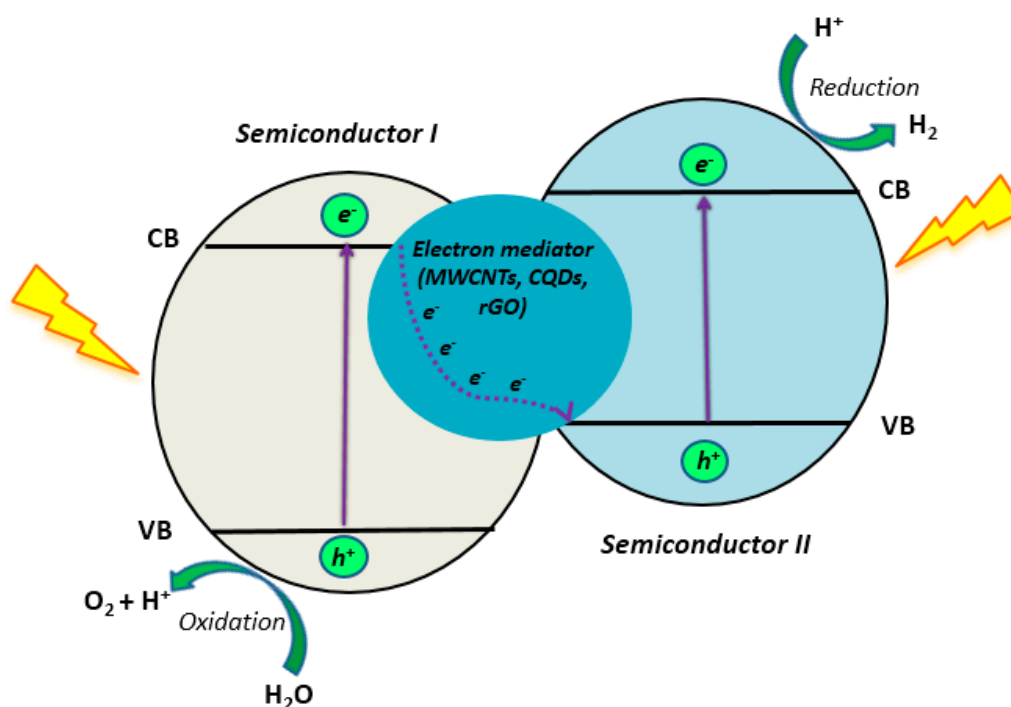


**Figure 16.** The type Z-heterojunction with the use of different solid electron mediators (multiwall carbon nanotubes (MWCNTs), carbon quantum dots (CQDs), rGO).

#### 4. Conclusions

TiO<sub>2</sub>-based photocatalytic technology represents a promising up-coming technology for both renewable energy generation and water purification applications. It is necessary to work on developing TiO<sub>2</sub>-based semiconductor materials, which are active under broader spectrum of solar light, overcoming the indicated disadvantages of the solely TiO<sub>2</sub> utilization, since TiO<sub>2</sub> as a photocatalytic material cannot be used alone due to its limitations such as activity only in UV light region and rapid recombination of photogenerated charge carriers.

TiO<sub>2</sub>-semiconductor coupling offers promising results in water purification, particularly for the degradation and mineralization of CECs. However, it is necessary to evaluate the toxicities of degradation intermediates of CEC to check the real efficiency of such composites. Furthermore, the immobilization of TiO<sub>2</sub>-Semiconductor composites to photocatalytic reaction membranes must be envisaged for further upscale opportunities.

Great progress has also been recorded in the development of TiO<sub>2</sub>-based heterojunction for the application in solar-driven photocatalytic hydrogen generation. By morphological control of the obtained composites, higher H<sub>2</sub> generation, as well as better light harvesting can be achieved. It is noticed that still a great deal of research is being conducted by the use of different noble-metal co-catalysts and sacrificial agents, which, although increasing the efficiency of the process, reduces its environmental friendliness and increases the performance cost. Accordingly, to allow for the practical deployment of such units, as well as commercialization, it is necessary to produce cost-effective systems that will consider economic impact assessment, including operation cost and energy consumption, and that will not require the use of costly co-catalysts and other substances that promote system performance.

**Author Contributions:** Conceptualization, H.K., F.F., and A.L.B.; writing—original draft preparation, K.P., F.M.d.R., H.K.; writing—review and editing, M.K., U.L.Š., D.D.D., F.F. and A.L.B. All authors have read and agreed to the published version of the manuscript.

**Funding:** This research was funded by projects: “Nano-sized Solar-active Catalysts for Environmental Technologies” (NaSCeNT, IP-2018-01-1982), Croatian Science Foundation, and “Water Purification and Energy

Conversion using Novel Composite Materials and Solar Irradiation" (KK.01.1.1.04.0001), European Structural and Investment Funds (Croatia)

**Conflicts of Interest:** The authors declare no conflict of interest.

## References

1. European Commission. Directive 2000/60/EC of the European Parliament and of the Council, of 23 October 2000. *Off. J. Eur. Communities* **2000**, *327*, 1–72.
2. Water JPI. Available online: <http://www.waterjpi.eu/mapping-agenda/strategic-re> (accessed on 12 December 2019).
3. European Commission. Energy Strategy. Available online: <https://ec.europa.eu/energy/en/topics/energy-strategy> (accessed on 12 December 2019).
4. Martin, M. *Alternative Energy Sources and Technologies*; Springer: Basel, Switzerland, 2016.
5. Hasan, M.M.; Allam, N.K. Unbiased spontaneous solar hydrogen production using stable TiO<sub>2</sub>-CuO composite nanofiber photocatalysts. *RSC Adv.* **2018**, *8*, 37219–37228. [[CrossRef](#)]
6. Fujishima, A.; Honda, K. Electrochemical Photolysis of Water at a Semiconductor Electrode. *Nature* **1972**, *238*, 37–38. [[CrossRef](#)] [[PubMed](#)]
7. Frank, S.N.; Bard, A.J. Heterogeneous photocatalytic oxidation of cyanide ion in aqueous solutions at TiO<sub>2</sub>. *J. Am. Chem. Soc.* **1977**, *99*, 303–304. [[CrossRef](#)]
8. Turchi, C.S.; Ollis, D.F. Photocatalytic degradation of organic water contaminants: Mechanisms involving hydroxyl radical attack. *J. Catal.* **1990**, *122*, 178–192. [[CrossRef](#)]
9. Chong, M.N.; Jin, B.; Chow, C.W.K.; Saint, C. Recent developments in photocatalytic water treatment technology: A review. *Water Res.* **2010**, *44*, 2997–3027. [[CrossRef](#)] [[PubMed](#)]
10. Pelaez, M.; Nolan, N.T.; Pillai, S.C.; Seery, M.K.; Falaras, P.; Kontos, A.G.; Dunlop, P.S.M.; Hamilton, J.W.J.; Byrne, J.A.; O'Shea, K.; et al. A review on the visible light active titanium dioxide photocatalysts for environmental applications. *Appl. Catal. B Environ.* **2012**, *125*, 331–349. [[CrossRef](#)]
11. Jafari, T.; Moharreri, E.; Amin, A.S.; Miao, R.; Song, W.; Suib, S.L. Photocatalytic water splitting—The untamed dream: A review of recent advances. *Molecules* **2016**, *21*, 900. [[CrossRef](#)]
12. Jing, D.; Guo, L.; Zhao, L.; Zhang, X.; Liu, H.; Li, M.; Shen, S.; Liu, G.; Hu, X.; Zhang, X.; et al. Efficient solar hydrogen production by photocatalytic water splitting: From fundamental study to pilot demonstration. *Int. J. Hydrogen Energy* **2010**, *35*, 7087–7097. [[CrossRef](#)]
13. Hafeez, H.Y.; Lakhera, S.K.; Bellamkonda, S.; Rao, G.R.; Shankar, M.V.; Bahnemann, D.W.; Neppolian, B. Construction of ternary hybrid layered reduced graphene oxide supported g-C<sub>3</sub>N<sub>4</sub>-TiO<sub>2</sub> nanocomposite and its photocatalytic hydrogen production activity. *Int. J. Hydrogen Energy* **2018**, *43*, 3892–3904. [[CrossRef](#)]
14. Schneider, J.; Matsuoka, M.; Takeuchi, M.; Zhang, J.; Horiuchi, Y.; Anpo, M.; Bahnemann, D.W. Understanding TiO<sub>2</sub> photocatalysis: Mechanisms and materials. *Chem. Rev.* **2014**, *114*, 9919–9986. [[CrossRef](#)] [[PubMed](#)]
15. Pichat, P. *Photocatalysis and Water Purification: From Fundamentals to Recent Applications*; Wiley: Weinheim, Germany, 2013.
16. Fagan, R.; McCormack, D.E.; Dionysiou, D.D.; Pillai, S.C. A review of solar and visible light active TiO<sub>2</sub> photocatalysis for treating bacteria, cyanotoxins and contaminants of emerging concern. *Mater. Sci. Semicond. Process.* **2016**, *42*, 2–14. [[CrossRef](#)]
17. Qi, K.; Cheng, B.; Yu, J.; Ho, W. A review on TiO<sub>2</sub> -based Z-scheme photocatalysts. *Chin. J. Catal.* **2017**, *38*, 1936–1955. [[CrossRef](#)]
18. Calvete, M.J.F.; Piccirillo, G.; Vinagreiro, C.S.; Pereira, M.M. Hybrid materials for heterogeneous photocatalytic degradation of antibiotics. *Coord. Chem. Rev.* **2019**, *395*, 63–85. [[CrossRef](#)]
19. Tong, H.; Ouyang, S.; Bi, Y.; Umezawa, N.; Oshikiri, M.; Ye, J. Nano-photocatalytic materials: Possibilities and challenges. *Adv. Mater.* **2012**, *24*, 229–251. [[CrossRef](#)] [[PubMed](#)]
20. Pasternak, S.; Paz, Y. On the similarity and dissimilarity between photocatalytic water splitting and photocatalytic degradation of pollutants. *ChemPhysChem* **2013**, *14*, 2059–2070. [[CrossRef](#)]
21. Wang, H.; Zhang, L.; Chen, Z.; Hu, J.; Li, S.; Wang, Z.; Liu, J.; Wang, X. Semiconductor heterojunction photocatalysts: Design, construction, and photocatalytic performances. *Chem. Soc. Rev.* **2014**, *43*, 5234–5244. [[CrossRef](#)]
22. Moniz, S.J.A.; Shevlin, S.A.; Martin, D.J.; Guo, Z.X.; Tang, J. Visible-light driven heterojunction photocatalysts for water splitting—a critical review. *Energy Environ. Sci.* **2015**, *8*, 731–759. [[CrossRef](#)]

23. Moniz, S.J.A.; Shevlin, S.A.; An, X.; Guo, Z.X.; Tang, J. Fe<sub>2</sub>O<sub>3</sub>-TiO<sub>2</sub> nanocomposites for enhanced charge separation and photocatalytic activity. *Chem. A Eur. J.* **2014**, *20*, 15571–15579. [[CrossRef](#)]
24. Macías-Tamez, R.; Villanueva-Rodríguez, M.; Ramos-Delgado, N.A.; Maya-Treviño, L.; Hernández-Ramírez, A. Comparative Study of the Photocatalytic Degradation of the Herbicide 2,4-D Using WO<sub>3</sub>/TiO<sub>2</sub> and Fe<sub>2</sub>O<sub>3</sub>/TiO<sub>2</sub> as Catalysts. *Water Air Soil Pollut.* **2017**, *228*, 379. [[CrossRef](#)]
25. Luo, L.; Long, J.; Zhao, S.; Dai, J.; Ma, L.; Wang, H.; Xia, L.; Shu, L.; Jiang, F. Effective visible-light-driven photocatalytic degradation of 17 $\alpha$ -ethynylestradiol by crosslinked CdS nano-rod/TiO<sub>2</sub> (B) nano-belt composite. *Process Saf. Environ. Prot.* **2019**, *130*, 77–85. [[CrossRef](#)]
26. Marschall, R. Semiconductor composites: Strategies for enhancing charge carrier separation to improve photocatalytic activity. *Adv. Funct. Mater.* **2014**, *24*, 2421–2440. [[CrossRef](#)]
27. Kaur, A.; Salunke, D.B.; Umar, A.; Mehta, S.K.; Sinha, A.S.K.; Kansal, S.K. Visible light driven photocatalytic degradation of fluoroquinolone levofloxacin drug using Ag<sub>2</sub>O/TiO<sub>2</sub> quantum dots: A mechanistic study and degradation pathway. *New J. Chem.* **2017**, *41*, 12079–12090. [[CrossRef](#)]
28. Gou, J.; Ma, Q.; Deng, X.; Cui, Y.; Zhang, H.; Cheng, X.; Li, X.; Xie, M.; Cheng, Q. Fabrication of Ag<sub>2</sub>O/TiO<sub>2</sub>-Zeolite composite and its enhanced solar light photocatalytic performance and mechanism for degradation of norfloxacin. *Chem. Eng. J.* **2017**, *308*, 818–826. [[CrossRef](#)]
29. Dong, P.; Hou, G.; Xi, X.; Shao, R.; Dong, F. WO<sub>3</sub>-based photocatalysts: Morphology control, activity enhancement and multifunctional applications. *Environ. Sci. Nano* **2017**, *4*, 539–557. [[CrossRef](#)]
30. Mugunthan, E.; Saidutta, M.B.; Jagadeeshbabu, P.E. Visible light assisted photocatalytic degradation of diclofenac using TiO<sub>2</sub>-WO<sub>3</sub> mixed oxide catalysts. *Environ. Nanotechnol. Monit. Manag.* **2018**, *10*, 322–330.
31. Cordero-García, A.; Turnes Palomino, G.; Hinojosa-Reyes, L.; Guzmán-Mar, J.L.; Maya-Treviño, L.; Hernández-Ramírez, A. Photocatalytic behaviour of WO<sub>3</sub>/TiO<sub>2</sub>-N for diclofenac degradation using simulated solar radiation as an activation source. *Environ. Sci. Pollut. Res.* **2017**, *24*, 4613–4624. [[CrossRef](#)]
32. Cordero-García, A.; Guzmán-Mar, J.L.; Hinojosa-Reyes, L.; Ruiz-Ruiz, E.; Hernández-Ramírez, A. Effect of carbon doping on WO<sub>3</sub>/TiO<sub>2</sub> coupled oxide and its photocatalytic activity on diclofenac degradation. *Ceram. Int.* **2016**, *42*, 9796–9803. [[CrossRef](#)]
33. Pérez-Estrada, L.A.; Malato, S.; Gernjak, W.; Agüera, A.; Thurman, E.M.; Ferrer, I.; Fernández-Alba, A.R. Photo-fenton degradation of diclofenac: Identification of main intermediates and degradation pathway. *Environ. Sci. Technol.* **2005**, *39*, 8300–8306. [[CrossRef](#)]
34. Salaeh, S.; Juretic Perisic, D.; Biosic, M.; Kusic, H.; Babic, S.; Lavrencic Stangar, U.; Dionysiou, D.D.; Loncaric Bozic, A. Diclofenac removal by simulated solar assisted photocatalysis using TiO<sub>2</sub>-based zeolite catalyst; mechanisms, pathways and environmental aspects. *Chem. Eng. J.* **2016**, *304*, 289–302. [[CrossRef](#)]
35. Arce-Sarria, A.; Machuca-Martínez, F.; Bustillo-Lecompte, C.; Hernández-Ramírez, A.; Colina-Márquez, J. Degradation and loss of antibacterial activity of commercial amoxicillin with TiO<sub>2</sub>/WO<sub>3</sub>-assisted solar photocatalysis. *Catalysts* **2018**, *8*, 222. [[CrossRef](#)]
36. Mishra, M.; Chun, D.M.  $\alpha$ -Fe<sub>2</sub>O<sub>3</sub> as a photocatalytic material: A review. *Appl. Catal. A Gen.* **2015**, *498*, 126–141. [[CrossRef](#)]
37. Mirmasoomi, S.R.; Mehdipour Ghazi, M.; Galedari, M. Photocatalytic degradation of diazinon under visible light using TiO<sub>2</sub>/Fe<sub>2</sub>O<sub>3</sub> nanocomposite synthesized by ultrasonic-assisted impregnation method. *Sep. Purif. Technol.* **2017**, *175*, 418–427. [[CrossRef](#)]
38. Li, R.; Liu, J.; Jia, Y.; Zhen, Q. Photocatalytic degradation mechanism of oxytetracyclines using Fe<sub>2</sub>O<sub>3</sub>-TiO<sub>2</sub> nanopowders. *J. Nanosci. Nanotechnol.* **2017**, *17*, 3010–3015. [[CrossRef](#)]
39. Li, R.; Jia, Y.; Wu, J.; Zhen, Q. Photocatalytic degradation and pathway of oxytetracycline in aqueous solution by Fe<sub>2</sub>O<sub>3</sub>-TiO<sub>2</sub> nanopowder. *RSC Adv.* **2015**, *5*, 40764–40771. [[CrossRef](#)]
40. Lu, C.; Guan, W.; Zhang, G.; Ye, L.; Zhou, Y.; Zhang, X. TiO<sub>2</sub>/Fe<sub>2</sub>O<sub>3</sub>/CNTs magnetic photocatalyst: A fast and convenient synthesis and visible-light-driven photocatalytic degradation of tetracycline. *Micro Nano Lett.* **2013**, *8*, 749–752. [[CrossRef](#)]
41. Zheng, X.; Fu, W.; Kang, F.; Peng, H.; Wen, J. Enhanced photo-Fenton degradation of tetracycline using TiO<sub>2</sub>-coated  $\alpha$ -Fe<sub>2</sub>O<sub>3</sub> core-shell heterojunction. *J. Ind. Eng. Chem.* **2018**, *68*, 14–23. [[CrossRef](#)]
42. Casbeer, E.; Sharma, V.K.; Li, X.Z. Synthesis and photocatalytic activity of ferrites under visible light: A review. *Sep. Purif. Technol.* **2012**, *87*, 1–14. [[CrossRef](#)]
43. Garcia-Muñoz, P.; Fresno, F.; de la Peña O'Shea, V.A.; Keller, N. Ferrite Materials for Photoassisted Environmental and Solar Fuels Applications. *Top. Curr. Chem.* **2020**, *378*, 6. [[CrossRef](#)]

44. Chen, Y.; Wu, Q.; Wang, J.; Song, Y. The fabrication of magnetic recyclable nitrogen-doped titanium dioxide/calcium ferrite/diatomite heterojunction nanocomposite for improved visible-light-driven degradation of tetracycline. *J. Chem. Technol. Biotechnol.* **2019**, *94*, 2702–2712. [[CrossRef](#)]
45. Chen, Y.; Liu, K. Fabrication of magnetically recyclable Ce/N co-doped TiO<sub>2</sub>/NiFe<sub>2</sub>O<sub>4</sub>/diatomite ternary hybrid: Improved photocatalytic efficiency under visible light irradiation. *J. Alloys Compd.* **2017**, *697*, 161–173. [[CrossRef](#)]
46. Wu, Q.; Zhang, Z. The fabrication of magnetic recyclable nitrogen modified titanium dioxide/strontium ferrite/diatomite heterojunction nanocomposite for enhanced visible-light-driven photodegradation of tetracycline. *Int. J. Hydrogen Energy* **2019**, *44*, 8261–8272. [[CrossRef](#)]
47. Nguyen, T.B.; Doong, R.A. Heterostructured ZnFe<sub>2</sub>O<sub>4</sub>/TiO<sub>2</sub> nanocomposites with a highly recyclable visible-light-response for bisphenol a degradation. *RSC Adv.* **2017**, *7*, 50006–50016. [[CrossRef](#)]
48. Shi, Y.; Yang, Z.; Wang, B.; An, H.; Chen, Z.; Cui, H. Adsorption and photocatalytic degradation of tetracycline hydrochloride using a palygorskite-supported Cu<sub>2</sub>O-TiO<sub>2</sub> composite. *Appl. Clay Sci.* **2016**, *119*, 311–320. [[CrossRef](#)]
49. Hu, Z.; Wang, X.; Dong, H.; Li, S.; Li, X.; Li, L. Efficient photocatalytic degradation of tetrabromodiphenyl ethers and simultaneous hydrogen production by TiO<sub>2</sub>-Cu<sub>2</sub>O composite films in N<sub>2</sub> atmosphere: Influencing factors, kinetics and mechanism. *J. Hazard. Mater.* **2017**, *340*, 1–15. [[CrossRef](#)]
50. Sud, D.; Syal, A. Investigations on the Phase Transformation, Optical Characteristics, and Photocatalytic Activity of Synthesized Heterostructured Nanoporous Bi<sub>2</sub>O<sub>3</sub>-TiO<sub>2</sub>. *J. Chin. Chem. Soc.* **2016**, *63*, 776–783. [[CrossRef](#)]
51. Sood, S.; Mehta, S.K.; Sinha, A.S.K.; Kansal, S.K. Bi<sub>2</sub>O<sub>3</sub>/TiO<sub>2</sub> heterostructures: Synthesis, characterization and their application in solar light mediated photocatalyzed degradation of an antibiotic, ofloxacin. *Chem. Eng. J.* **2016**, *290*, 45–52. [[CrossRef](#)]
52. Kaur, A.; Umar, A.; Anderson, W.A.; Kansal, S.K. Facile synthesis of CdS/TiO<sub>2</sub> nanocomposite and their catalytic activity for ofloxacin degradation under visible illumination. *J. Photochem. Photobiol. A Chem.* **2018**, *360*, 34–43. [[CrossRef](#)]
53. Kušić, H.; Leszczynska, D. Altered toxicity of organic pollutants in water originated from simultaneous exposure to UV photolysis and CdSe/ZnS quantum dots. *Chemosphere* **2012**, *89*, 900–906. [[CrossRef](#)]
54. Ning, X.; Li, J.; Yang, B.; Zhen, W.; Li, Z.; Tian, B.; Lu, G. Inhibition of photocorrosion of CdS via assembling with thin film TiO<sub>2</sub> and removing formed oxygen by artificial gill for visible light overall water splitting. *Appl. Catal. B Environ.* **2017**, *212*, 129–139. [[CrossRef](#)]
55. Pan, Y.X.; Zhou, T.; Han, J.; Hong, J.; Wang, Y.; Zhang, W.; Xu, R. CdS quantum dots and tungsten carbide supported on anatase-rutile composite TiO<sub>2</sub> for highly efficient visible-light-driven photocatalytic H<sub>2</sub> evolution from water. *Catal. Sci. Technol.* **2016**, *6*, 2206–2213. [[CrossRef](#)]
56. Zhu, R.; Yang, R.; Hu, L.; Chen, B. Preparation of Z-Scheme system of CdS-RGO-BiVO<sub>4</sub> and its activity for hydrogen production. *Int. J. Hydrogen Energy* **2019**, *44*, 25119–25128. [[CrossRef](#)]
57. Kandi, D.; Behera, A.; Martha, S.; Naik, B.; Parida, K.M. Quantum confinement chemistry of CdS QDs plus hot electron of Au over TiO<sub>2</sub> nanowire protruding to be encouraging photocatalyst towards nitrophenol conversion and ciprofloxacin degradation. *J. Environ. Chem. Eng.* **2019**, *7*, 102821. [[CrossRef](#)]
58. Li, W.; Ding, H.; Ji, H.; Dai, W.; Guo, J.; Du, G. Photocatalytic degradation of tetracycline hydrochloride via a CdS-TiO<sub>2</sub> heterostructure composite under visible light irradiation. *Nanomaterials* **2018**, *8*, 415. [[CrossRef](#)]
59. Jiang, Y.; Zhang, M.; Xin, Y.; Chai, C.; Chen, Q. Construction of immobilized CuS/TiO<sub>2</sub> nanobelts heterojunction photocatalyst for photocatalytic degradation of enrofloxacin: Synthesis, characterization, influencing factors and mechanism insight. *J. Chem. Technol. Biotechnol.* **2019**, *94*, 2219–2228.
60. Chen, Q.; Wu, S.; Xin, Y. Synthesis of Au-CuS-TiO<sub>2</sub> nanobelts photocatalyst for efficient photocatalytic degradation of antibiotic oxytetracycline. *Chem. Eng. J.* **2016**, *302*, 377–387. [[CrossRef](#)]
61. Irandost, M.; Akbarzadeh, R.; Pirsaeheb, M.; Asadi, A.; Mohammadi, P.; Sillanpää, M. Fabrication of highly visible active N, S co-doped TiO<sub>2</sub>@MoS<sub>2</sub> heterojunction with synergistic effect for photocatalytic degradation of diclofenac: Mechanisms, modeling and degradation pathway. *J. Mol. Liq.* **2019**, *291*, 111342. [[CrossRef](#)]
62. Wu, L.; Shi, S.; Li, Q.; Zhang, X.; Cui, X. TiO<sub>2</sub> nanoparticles modified with 2D MoSe<sub>2</sub> for enhanced photocatalytic activity on hydrogen evolution. *Int. J. Hydrogen Energy* **2019**, *44*, 720–728. [[CrossRef](#)]

63. Du, J.; Wang, H.; Yang, M.; Zhang, F.; Wu, H.; Cheng, X.; Yuan, S.; Zhang, B.; Li, K.; Wang, Y.; et al. Highly efficient hydrogen evolution catalysis based on MoS<sub>2</sub>/CdS/TiO<sub>2</sub> porous composites. *Int. J. Hydrogen Energy* **2018**, *43*, 9307–9315. [[CrossRef](#)]
64. Kumar, N.; Bhadwal, A.S.; Mizaikoff, B.; Singh, S.; Kranz, C. Electrochemical detection and photocatalytic performance of MoS<sub>2</sub>/TiO<sub>2</sub> nanocomposite against pharmaceutical contaminant: Paracetamol. *Sens. Bio-Sens. Res.* **2019**, *24*, 100288. [[CrossRef](#)]
65. Deng, L.; Liu, H.; Gao, X.; Su, X.; Zhu, Z. SnS<sub>2</sub>/TiO<sub>2</sub> nanocomposites with enhanced visible light-driven photoreduction of aqueous Cr(VI). *Ceram. Int.* **2016**, *42*, 3808–3815. [[CrossRef](#)]
66. Kovacic, M.; Kopicic, N.; Kusic, H.; Bozic, A.L. Solar driven degradation of 17β-estradiol using composite photocatalytic materials and artificial irradiation source: Influence of process and water matrix parameters. *J. Photochem. Photobiol. A Chem.* **2018**, *361*, 48–61. [[CrossRef](#)]
67. Kovacic, M.; Papac, J.; Kusic, H.; Karamanis, P.; Loncaric Bozic, A. Degradation of polar and non-polar pharmaceutical pollutants in water by solar assisted photocatalysis using hydrothermal TiO<sub>2</sub>-SnS<sub>2</sub>. *Chem. Eng. J.* **2019**, *382*, 122826. [[CrossRef](#)]
68. Yan, T.; Guan, W.; Li, W.; You, J. Ag<sub>3</sub>PO<sub>4</sub> photocatalysts loaded on uniform SiO<sub>2</sub> supports for efficient degradation of methyl orange under visible light irradiation. *RSC Adv.* **2014**, *4*, 37095–37099. [[CrossRef](#)]
69. Yi, Z.; Ye, J.; Kikugawa, N.; Kako, T.; Ouyang, S.; Stuart-Williams, H.; Yang, H.; Cao, J.; Luo, W.; Li, Z.; et al. An orthophosphate semiconductor with photooxidation properties under visible-light irradiation. *Nat. Mater.* **2010**, *9*, 559–564. [[CrossRef](#)]
70. Ren, J.; Chai, Y.; Liu, Q.; Zhang, L.; Dai, W.L. Intercorrelated Ag<sub>3</sub>PO<sub>4</sub> nanoparticles decorated with graphitic carbon nitride: Enhanced stability and photocatalytic activities for water treatment. *Appl. Surf. Sci.* **2017**, *403*, 177–186. [[CrossRef](#)]
71. Meng, S.; Ning, X.; Zhang, T.; Chen, S.F.; Fu, X. What is the transfer mechanism of photogenerated carriers for the nanocomposite photocatalyst Ag<sub>3</sub>PO<sub>4</sub>/g-C<sub>3</sub>N<sub>4</sub>, band-band transfer or a direct Z-scheme? *Phys. Chem. Chem. Phys.* **2015**, *17*, 11577–11585. [[CrossRef](#)]
72. Wang, Y.; Yu, H.; Lu, Y.; Qu, J.; Zhu, S.; Huo, M. A nano-composite comprised of Ti<sup>3+</sup>-doped TiO<sub>2</sub> nanotubes and Ag<sub>3</sub>PO<sub>4</sub> quantum dots with enhanced photocatalytic activity under visible light. *Mater. Lett.* **2019**, *240*, 35–38. [[CrossRef](#)]
73. Du, J.; Ma, S.; Yan, Y.; Li, K.; Zhao, F.; Zhou, J. Corn-silk-templated synthesis of TiO<sub>2</sub> nanotube arrays with Ag<sub>3</sub>PO<sub>4</sub> nanoparticles for efficient oxidation of organic pollutants and pathogenic bacteria under solar light. *Colloids Surf. A Physicochem. Eng. Asp.* **2019**, *572*, 237–249. [[CrossRef](#)]
74. Liu, J.; Xie, F.; Li, R.; Li, T.; Jia, Z.; Wang, Y.; Wang, Y.; Zhang, X.; Fan, C. TiO<sub>2-x</sub>/Ag<sub>3</sub>PO<sub>4</sub> photocatalyst: Oxygen vacancy dependent visible light photocatalytic performance and BPA degradative pathway. *Mater. Sci. Semicond. Process.* **2019**, *97*, 1–10. [[CrossRef](#)]
75. Police, A.K.R.; Chennaiahgari, M.; Boddula, R.; Vattikuti, S.V.P.; Mandari, K.K.; Chan, B. Single-step hydrothermal synthesis of wrinkled graphene wrapped TiO<sub>2</sub> nanotubes for photocatalytic hydrogen production and supercapacitor applications. *Mater. Res. Bull.* **2018**, *98*, 314–321. [[CrossRef](#)]
76. Lu, Y.; Ma, B.; Yang, Y.; Huang, E.; Ge, Z.; Zhang, T.; Zhang, S.; Li, L.; Guan, N.; Ma, Y.; et al. High activity of hot electrons from bulk 3D graphene materials for efficient photocatalytic hydrogen production. *Nano Res.* **2017**, *10*, 1662–1672. [[CrossRef](#)]
77. Hao, X.; Li, M.; Zhang, L.; Wang, K.; Liu, C. Photocatalyst TiO<sub>2</sub>/WO<sub>3</sub>/GO nano-composite with high efficient photocatalytic performance for BPA degradation under visible light and solar light illumination. *J. Ind. Eng. Chem.* **2017**, *55*, 140–148. [[CrossRef](#)]
78. Wang, G.; Chen, Q.; Xin, Y.; Liu, Y.; Zang, Z.; Hu, C.; Zhang, B. Construction of graphene-WO<sub>3</sub>/TiO<sub>2</sub> nanotube array photoelectrodes and its enhanced performance for photocatalytic degradation of dimethyl phthalate. *Electrochim. Acta* **2016**, *222*, 1903–1913. [[CrossRef](#)]
79. Bilgin Simsek, E.; Kilic, B.; Asgin, M.; Akan, A. Graphene oxide based heterojunction TiO<sub>2</sub>-ZnO catalysts with outstanding photocatalytic performance for bisphenol-A, ibuprofen and flurbiprofen. *J. Ind. Eng. Chem.* **2018**, *59*, 115–126. [[CrossRef](#)]
80. Feng, J.; Wang, Y.; Hou, Y.; Li, L. Hierarchical structured ZnFe<sub>2</sub>O<sub>4</sub>@RGO@TiO<sub>2</sub> composite as powerful visible light catalyst for degradation of fulvic acid. *J. Nanopart. Res.* **2017**, *19*, 178. [[CrossRef](#)]

81. Luo, L.j.; Li, J.; Dai, J.; Xia, L.; Barrow, C.J.; Wang, H.; Jegatheesan, J.; Yang, M. Bisphenol A removal on TiO<sub>2</sub>-MoS<sub>2</sub>-reduced graphene oxide composite by adsorption and photocatalysis. *Process Saf. Environ. Prot.* **2017**, *112*, 274–279. [[CrossRef](#)]
82. Wang, W.; Han, Q.; Zhu, Z.; Zhang, L.; Zhong, S.; Liu, B. Enhanced photocatalytic degradation performance of organic contaminants by heterojunction photocatalyst BiVO<sub>4</sub>/TiO<sub>2</sub>/RGO and its compatibility on four different tetracycline antibiotics. *Adv. Powder Technol.* **2019**, *30*, 1882–1896. [[CrossRef](#)]
83. Alcudia-Ramos, M.A.; Fuentez-Torres, M.O.; Ortiz-Chi, F.; Espinosa-González, C.G.; Hernández-Como, N.; García-Zaleta, D.S.; Kesarla, M.K.; Torres-Torres, J.G.; Collins-Martínez, V.; Godavarthi, S. Fabrication of g-C<sub>3</sub>N<sub>4</sub>/TiO<sub>2</sub> heterojunction composite for enhanced photocatalytic hydrogen production. *Ceram. Int.* **2020**, *46*, 38–45. [[CrossRef](#)]
84. Liu, C.; Wu, P.; Wu, J.; Hou, J.; Bai, H.; Liu, Z. Effective protect of oxygen vacancies in carbon layer coated black TiO<sub>2-x</sub>/CNNS hetero-junction photocatalyst. *Chem. Eng. J.* **2019**, *359*, 58–68. [[CrossRef](#)]
85. Yang, Y.; Li, X.; Lu, C.; Huang, W. G-C<sub>3</sub>N<sub>4</sub> Nanosheets Coupled with TiO<sub>2</sub> Nanosheets as 2D/2D Heterojunction Photocatalysts Toward High Photocatalytic Activity for Hydrogen Production. *Catal. Lett.* **2019**, *140*, 2930–2939. [[CrossRef](#)]
86. Kong, L.; Zhang, X.; Wang, C.; Xu, J.; Du, X.; Li, L. Ti<sup>3+</sup> defect mediated g-C<sub>3</sub>N<sub>4</sub>/TiO<sub>2</sub> Z-scheme system for enhanced photocatalytic redox performance. *Appl. Surf. Sci.* **2018**, *448*, 288–296. [[CrossRef](#)]
87. Wang, J.; Wang, G.; Wang, X.; Wu, Y.; Su, Y.; Tang, H. 3D/2D direct Z-scheme heterojunctions of hierarchical TiO<sub>2</sub> microflowers/g-C<sub>3</sub>N<sub>4</sub> nanosheets with enhanced charge carrier separation for photocatalytic H<sub>2</sub> evolution. *Carbon* **2019**, *149*, 618–626. [[CrossRef](#)]
88. Pan, C.; Jia, J.; Hu, X.; Fan, J.; Liu, E. In situ construction of g-C<sub>3</sub>N<sub>4</sub>/TiO<sub>2</sub> heterojunction films with enhanced photocatalytic activity over magnetic-driven rotating frame. *Appl. Surf. Sci.* **2018**, *430*, 283–292. [[CrossRef](#)]
89. Zou, Y.; Shi, J.W.; Ma, D.; Fan, Z.; Lu, L.; Niu, C. In situ synthesis of C-doped TiO<sub>2</sub>@g-C<sub>3</sub>N<sub>4</sub> core-shell hollow nanospheres with enhanced visible-light photocatalytic activity for H<sub>2</sub> evolution. *Chem. Eng. J.* **2017**, *322*, 435–444. [[CrossRef](#)]
90. Ma, J.; Zhou, W.; Tan, X.; Yu, T. Potassium ions intercalated into g-C<sub>3</sub>N<sub>4</sub>-modified TiO<sub>2</sub> nanobelts for the enhancement of photocatalytic hydrogen evolution activity under visible-light irradiation. *Nanotechnology* **2018**, *29*, 215706. [[CrossRef](#)]
91. Pan, J.; You, M.; Chi, C.; Dong, Z.; Wang, B.; Zhu, M.; Zhao, W.; Song, C.; Zheng, Y.; Li, C. The two dimension carbon quantum dots modified porous g-C<sub>3</sub>N<sub>4</sub>/TiO<sub>2</sub> nano-heterojunctions for visible light hydrogen production enhancement. *Int. J. Hydrogen Energy* **2018**, *43*, 6586–6593. [[CrossRef](#)]
92. Wang, X.; Maeda, K.; Thomas, A.; Takane, K.; Xin, G.; Carlsson, J.M.; Domen, K.; Antonietti, M. A metal-free polymeric photocatalyst for hydrogen production from water under visible light. *Nat. Mater.* **2009**, *8*, 76–80. [[CrossRef](#)]
93. Corredor, J.; Rivero, M.J.; Rangel, C.M.; Gloaguen, F.; Ortiz, I. Comprehensive review and future perspectives on the photocatalytic hydrogen production. *J. Chem. Technol. Biotechnol.* **2019**, *94*, 3049–3063. [[CrossRef](#)]
94. Wen, J.; Xie, J.; Chen, X.; Li, X. A review on g-C<sub>3</sub>N<sub>4</sub>-based photocatalysts. *Appl. Surf. Sci.* **2017**, *391*, 72–123. [[CrossRef](#)]
95. Huang, H.; He, M.; Yang, X.; Tian, Z.; Hu, J.; Wen, B. One-pot hydrothermal synthesis of TiO<sub>2</sub>/RCN heterojunction photocatalyst for production of hydrogen and rhodamine B degradation. *Appl. Surf. Sci.* **2019**, *493*, 202–211. [[CrossRef](#)]
96. Yang, Z.; Yan, J.; Lian, J.; Xu, H.; She, X.; Li, H. g-C<sub>3</sub>N<sub>4</sub>/TiO<sub>2</sub> Nanocomposites for Degradation of Ciprofloxacin under Visible Light Irradiation. *ChemistrySelect* **2016**, *1*, 5679–5685. [[CrossRef](#)]
97. Li, G.; Nie, X.; Gao, Y.; An, T. Can environmental pharmaceuticals be photocatalytically degraded and completely mineralized in water using g-C<sub>3</sub>N<sub>4</sub>/TiO<sub>2</sub> under visible light irradiation?—Implications of persistent toxic intermediates. *Appl. Catal. B Environ.* **2016**, *180*, 726–732. [[CrossRef](#)]
98. Yu, S.; Wang, Y.; Sun, F.; Wang, R.; Zhou, Y. Novel mpg-C<sub>3</sub>N<sub>4</sub>/TiO<sub>2</sub> nanocomposite photocatalytic membrane reactor for sulfamethoxazole photodegradation. *Chem. Eng. J.* **2018**, *337*, 183–192. [[CrossRef](#)]
99. Wang, W.; Fang, J.; Shao, S.; Lai, M.; Lu, C. Compact and uniform TiO<sub>2</sub>@g-C<sub>3</sub>N<sub>4</sub> core-shell quantum heterojunction for photocatalytic degradation of tetracycline antibiotics. *Appl. Catal. B Environ.* **2017**, *217*, 57–64. [[CrossRef](#)]



100. Li, C.; Sun, Z.; Zhang, W.; Yu, C.; Zheng, S. Highly efficient g-C<sub>3</sub>N<sub>4</sub>/TiO<sub>2</sub>/kaolinite composite with novel three-dimensional structure and enhanced visible light responding ability towards ciprofloxacin and S. aureus. *Appl. Catal. B Environ.* **2018**, *220*, 272–282. [[CrossRef](#)]
101. Chen, Y.; Lu, W.; Shen, H.; Gu, Y.; Xu, T.; Zhu, Z.; Wang, G.; Chen, W. Solar-driven efficient degradation of emerging contaminants by g-C<sub>3</sub>N<sub>4</sub>-shielding polyester fiber/TiO<sub>2</sub> composites. *Appl. Catal. B Environ.* **2019**, *258*, 117960. [[CrossRef](#)]
102. Xie, X.; Chen, C.; Wang, X.; Li, J.; Naraginti, S. Efficient detoxification of triclosan by a S-Ag/TiO<sub>2</sub>@g-C<sub>3</sub>N<sub>4</sub> hybrid photocatalyst: Process optimization and bio-toxicity assessment. *RSC Adv.* **2019**, *9*, 20439–20449. [[CrossRef](#)]
103. Song, J.; Wu, X.; Zhang, M.; Liu, C.; Yu, J.; Sun, G.; Si, Y.; Ding, B. Highly flexible, core-shell heterostructured, and visible-light-driven titania-based nanofibrous membranes for antibiotic removal and E. coil inactivation. *Chem. Eng. J.* **2020**, *379*, 122269. [[CrossRef](#)]
104. Yang, L.; Bai, X.; Shi, J.; Du, X.; Xu, L.; Jin, P. Quasi-full-visible-light absorption by D35-TiO<sub>2</sub>/g-C<sub>3</sub>N<sub>4</sub> for synergistic persulfate activation towards efficient photodegradation of micropollutants. *Appl. Catal. B Environ.* **2019**, *256*, 117759. [[CrossRef](#)]
105. Su, Y.; Chen, P.; Wang, F.; Zhang, Q.; Chen, T.; Wang, Y.; Yao, K.; Lv, W.; Liu, G. Decoration of TiO<sub>2</sub>/g-C<sub>3</sub>N<sub>4</sub> Z-scheme by carbon dots as a novel photocatalyst with improved visible-light photocatalytic performance for the degradation of enrofloxacin. *RSC Adv.* **2017**, *7*, 34096–34103. [[CrossRef](#)]
106. Wang, F.; Chen, P.; Feng, Y.; Xie, Z.; Liu, Y.; Su, Y.; Zhang, Q.; Wang, Y.; Yao, K.; Lv, W.; et al. Facile synthesis of N-doped carbon dots/g-C<sub>3</sub>N<sub>4</sub> photocatalyst with enhanced visible-light photocatalytic activity for the degradation of indomethacin. *Appl. Catal. B Environ.* **2017**, *207*, 103–113. [[CrossRef](#)]
107. Nie, Y.C.; Yu, F.; Wang, L.C.; Xing, Q.J.; Liu, X.; Pei, Y.; Zou, J.P.; Dai, W.L.; Li, Y.; Suib, S.L. Photocatalytic degradation of organic pollutants coupled with simultaneous photocatalytic H<sub>2</sub> evolution over graphene quantum dots/Mn-N-TiO<sub>2</sub>/g-C<sub>3</sub>N<sub>4</sub> composite catalysts: Performance and mechanism. *Appl. Catal. B Environ.* **2018**, *227*, 312–321. [[CrossRef](#)]
108. Jo, W.K.; Adinaveen, T.; Vijaya, J.J.; Sagaya Selvam, N.C. Synthesis of MoS<sub>2</sub> nanosheet supported Z-scheme TiO<sub>2</sub>/g-C<sub>3</sub>N<sub>4</sub> photocatalysts for the enhanced photocatalytic degradation of organic water pollutants. *RSC Adv.* **2016**, *6*, 10487–10497.
109. Tahir, M.B.; Sagir, M.; Shahzad, K. Removal of acetylsalicylate and methyl-theobromine from aqueous environment using nano-photocatalyst WO<sub>3</sub>-TiO<sub>2</sub> @g-C<sub>3</sub>N<sub>4</sub> composite. *J. Hazard. Mater.* **2019**, *363*, 205–213. [[CrossRef](#)]
110. Schubert, J.S.; Popovic, J.; Haselmann, G.M.; Nandan, S.P.; Wang, J.; Giesriegl, A.; Cherevan, A.S.; Eder, D. Immobilization of Co, Mn, Ni and Fe oxide co-catalysts on TiO<sub>2</sub> for photocatalytic water splitting reactions. *J. Mater. Chem. A* **2019**, *7*, 18568–18579. [[CrossRef](#)]
111. Patil, S.B.; Basavarajappa, P.S.; Ganganagappa, N.; Jyothi, M.S.; Raghu, A.V.; Reddy, K.R. Recent advances in non-metals-doped TiO<sub>2</sub> nanostructured photocatalysts for visible-light driven hydrogen production, CO<sub>2</sub> reduction and air purification. *Int. J. Hydrogen Energy* **2019**, *44*, 13022–13039. [[CrossRef](#)]
112. Yang, Q.; Dong, L.; Su, R.; Hu, B.; Wang, Z.; Jin, Y.; Wang, Y.; Besenbacher, F.; Dong, M. Nanostructured heterogeneous photo-catalysts for hydrogen production and water splitting: A comprehensive insight. *Appl. Mater. Today* **2019**, *17*, 159–182. [[CrossRef](#)]
113. Bhagya, T.C.; Krishnan, A.; Arunima Rajan, S.; Ameen Sha, M.; Sreelekshmy, B.R.; Jineesh, P.; Shibli, S.M.A. Exploration and evaluation of proton source-assisted photocatalyst for hydrogen generation. *Photochem. Photobiol. Sci.* **2019**, *18*, 1716–1726. [[CrossRef](#)]
114. Hernández-Majalca, B.C.; Meléndez-Zaragoza, M.J.; Salinas-Gutiérrez, J.M.; López-Ortiz, A.; Collins-Martínez, V. Visible-light photo-assisted synthesis of GO-TiO<sub>2</sub> composites for the photocatalytic hydrogen production. *Int. J. Hydrogen Energy* **2019**, *44*, 12381–12389. [[CrossRef](#)]
115. Wang, D.; Saleh, N.B.; Sun, W.; Park, C.M.; Shen, C.; Aich, N.; Peijnenburg, W.J.G.M.; Zhang, W.; Jin, Y.; Su, C. Next-Generation Multifunctional Carbon–Metal Nanohybrids for Energy and Environmental Applications. *Environ. Sci. Technol.* **2019**, *53*, 7265–7287. [[CrossRef](#)] [[PubMed](#)]
116. Xu, X.; Ray, R.; Gu, Y.; Ploehn, H.J.; Gearheart, L.; Raker, K.; Scrivens, W.A. Electrophoretic analysis and purification of fluorescent single-walled carbon nanotube fragments. *J. Am. Chem. Soc.* **2004**, *126*, 12736–12737. [[CrossRef](#)] [[PubMed](#)]

117. Rao, V.N.; Reddy, N.L.; Kumari, M.M.; Cheralathan, K.K.; Ravi, P.; Sathish, M.; Neppolian, B.; Reddy, K.R.; Shetti, N.P.; Prathap, P.; et al. Sustainable hydrogen production for the greener environment by quantum dots-based efficient photocatalysts: A review. *J. Environ. Manag.* **2019**, *248*, 109246. [[CrossRef](#)]
118. Yi, L.; Lan, F.; Li, J.; Zhao, C. Efficient Noble-Metal-Free Co-NG/TiO<sub>2</sub> Photocatalyst for H<sub>2</sub> Evolution: Synergistic Effect between Single-Atom Co and N-Doped Graphene for Enhanced Photocatalytic Activity. *ACS Sustain. Chem. Eng.* **2018**, *6*, 12766–12775. [[CrossRef](#)]
119. Rabin, N.N.; Ohmagari, H.; Islam, M.S.; Karim, M.R.; Hayami, S. A procession on photocatalyst for solar fuel production and waste treatment. *J. Incl. Phenom. Macrocycl. Chem.* **2019**, *94*, 263–281. [[CrossRef](#)]
120. Lv, T.; Wang, H.; Hong, W.; Wang, P.; Jia, L. In situ self-assembly synthesis of sandwich-like TiO<sub>2</sub>/reduced graphene oxide/LaFeO<sub>3</sub> Z-scheme ternary heterostructure towards enhanced photocatalytic hydrogen production. *Mol. Catal.* **2019**, *475*, 110497. [[CrossRef](#)]
121. Iwase, A.; Ng, Y.H.; Ishiguro, Y.; Kudo, A.; Amal, R. Reduced Graphene Oxide as a Solid-State Electron Mediator in Z-Scheme Photocatalytic Water Splitting under Visible Light. *J. Am. Chem. Soc.* **2011**, *133*, 11054–11057. [[CrossRef](#)]
122. Samal, A.; Das, D.P. Transfiguring UV light active “metal oxides” to visible light active photocatalyst by reduced graphene oxide hypostatization. *Catal. Today* **2018**, *300*, 124–135. [[CrossRef](#)]
123. Ida, S.; Wilson, P.; Neppolian, B.; Sathish, M.; Karthik, P.; Ravi, P. Ultrasonically aided selective stabilization of pyrrolic type nitrogen by one pot nitrogen doped and hydrothermally reduced Graphene oxide/Titania nanocomposite (N-TiO<sub>2</sub>/N-RGO) for H<sub>2</sub> production. *Ultrason. Sonochem.* **2019**, *57*, 62–72. [[CrossRef](#)]
124. Olowoyo, J.O.; Kumar, M.; Jain, S.L.; Babalola, J.O.; Vorontsov, A.V.; Kumar, U. Insights into Reinforced Photocatalytic Activity of the CNT-TiO<sub>2</sub> Nanocomposite for CO<sub>2</sub> Reduction and Water Splitting. *J. Phys. Chem. C* **2019**, *123*, 367–378. [[CrossRef](#)]
125. Umer, M.; Tahir, M.; Azam, M.U.; Tahir, B.; Jaffar, M.M.; Alias, H. Montmorillonite dispersed single wall carbon nanotubes (SWCNTs)/TiO<sub>2</sub> heterojunction composite for enhanced dynamic photocatalytic H<sub>2</sub> production under visible light. *Appl. Clay Sci.* **2019**, *174*, 110–119. [[CrossRef](#)]
126. Bellamkonda, S.; Thangavel, N.; Hafeez, H.Y.; Neppolian, B.; Ranga Rao, G. Highly active and stable multi-walled carbon nanotubes-graphene-TiO<sub>2</sub> nanohybrid: An efficient non-noble metal photocatalyst for water splitting. *Catal. Today* **2019**, *321*, 120–127. [[CrossRef](#)]
127. Haque, F.; Daeneke, T.; Kalantar-zadeh, K.; Ou, J.Z. Two-Dimensional Transition Metal Oxide and Chalcogenide-Based Photocatalysts. *Nano-Micro Lett.* **2018**, *10*, 23. [[CrossRef](#)] [[PubMed](#)]
128. Camposeco, R.; Castillo, S.; Rodriguez-González, V.; Hinojosa-Reyes, M.; Medina-Álvares, M.I.; Mejía-Centeno, I. Promotional effect of Rh nanoparticles on WO<sub>3</sub>/TiO<sub>2</sub> titanate nanotube photocatalysts for boosted hydrogen production. *J. Photochem. Photobiol. A Chem.* **2018**, *353*, 114–121. [[CrossRef](#)]
129. Ren, X.; Gao, P.; Kong, X.; Jiang, R.; Yang, P.; Chen, Y.; Chi, Q.; Li, B. NiO/Ni/TiO<sub>2</sub> nanocables with Schottky/p-n heterojunctions and the improved photocatalytic performance in water splitting under visible light. *J. Colloid Interface Sci.* **2018**, *530*, 1–8. [[CrossRef](#)] [[PubMed](#)]
130. Madhumitha, A.; Preethi, V.; Kanmani, S. Photocatalytic hydrogen production using TiO<sub>2</sub> coated iron-oxide core shell particles. *Int. J. Hydrogen Energy* **2018**, *43*, 3946–3956. [[CrossRef](#)]
131. Xie, M.Y.; Su, K.Y.; Peng, X.Y.; Wu, R.J.; Chavali, M.; Chang, W.C. Hydrogen production by photocatalytic water-splitting on Pt-doped TiO<sub>2</sub>-ZnO under visible light. *J. Taiwan Inst. Chem. Eng.* **2017**, *70*, 161–167. [[CrossRef](#)]
132. Chen, Q.; Tong, R.; Chen, X.; Xue, Y.; Xie, Z.; Kuang, Q.; Zheng, L. Ultrafine ZnO quantum dot-modified TiO<sub>2</sub> composite photocatalysts: The role of the quantum size effect in heterojunction-enhanced photocatalytic hydrogen evolution. *Catal. Sci. Technol.* **2018**, *8*, 1296–1303. [[CrossRef](#)]
133. Liu, J.; Ke, J.; Li, Y.; Liu, B.; Wang, L.; Xiao, H.; Wang, S. Co<sub>3</sub>O<sub>4</sub> quantum dots/TiO<sub>2</sub> nanobelt hybrids for highly efficient photocatalytic overall water splitting. *Appl. Catal. B Environ.* **2018**, *236*, 396–403. [[CrossRef](#)]
134. Zhang, Q.; Hai, Z.; Jian, A.; Xu, H.; Xue, C.; Sang, S. Synthesis of p-Co<sub>3</sub>O<sub>4</sub>/n-TiO<sub>2</sub> nanoparticles for overall water splitting under visible light irradiation. *Nanomaterials* **2016**, *6*, 138. [[CrossRef](#)]
135. Wang, L.; Zhang, X.; Gao, H.; Hu, J.; Mao, J.; Liang, C.; Zhang, P.; Shao, G. 3D CuO network supported TiO<sub>2</sub> nanosheets with applications for energy storage and water splitting. *Sci. Adv. Mater.* **2016**, *8*, 1256–1262. [[CrossRef](#)]
136. Wei, T.; Zhu, Y.-N.; An, X.; Liu, L.-M.; Cao, X.; Liu, H.; Qu, J. Defect Modulation of Z-Scheme TiO<sub>2</sub>/Cu<sub>2</sub>O Photocatalysts for Durable Water Splitting. *ACS Catal.* **2019**, *9*, 8346–8354. [[CrossRef](#)]

137. Rao, V.N.; Reddy, N.L.; Kumari, M.M.; Ravi, P.; Sathish, M.; Neppolian, B.; Shankar, M.V. Synthesis of titania wrapped cadmium sulfide nanorods for photocatalytic hydrogen generation. *Mater. Res. Bull.* **2018**, *103*, 122–132. [[CrossRef](#)]
138. Du, J.; Wang, H.; Yang, M.; Li, K.; Zhao, L.; Zhao, G.; Li, S.; Gu, X.; Zhou, Y.; Wang, L.; et al. Pyramid-like CdS nanoparticles grown on porous TiO<sub>2</sub> monolith: An advanced photocatalyst for H<sub>2</sub> production. *Electrochim. Acta* **2017**, *250*, 99–107. [[CrossRef](#)]
139. Peng, R.; Wu, C.M.; Baltrusaitis, J.; Dimitrijevic, N.M.; Rajh, T.; Koodali, R.T. Solar hydrogen generation over CdS incorporated in Ti-MCM-48 mesoporous materials under visible light illumination. *Int. J. Hydrogen Energy* **2016**, *41*, 4106–4119. [[CrossRef](#)]
140. Zhao, D.; Yang, C.F. Recent advances in the TiO<sub>2</sub>/CdS nanocomposite used for photocatalytic hydrogen production and quantum-dot-sensitized solar cells. *Renew. Sustain. Energy Rev.* **2016**, *54*, 1048–1059. [[CrossRef](#)]
141. Qi, L.; Yu, J.; Jaroniec, M. Preparation and enhanced visible-light photocatalytic H<sub>2</sub>- production activity of CdS-sensitized Pt/TiO<sub>2</sub> nanosheets with exposed (001) facets. *Phys. Chem. Chem. Phys.* **2011**, *13*, 8915–8923. [[CrossRef](#)]
142. Li, C.; Yuan, J.; Han, B.; Jiang, L.; Shangguan, W. TiO<sub>2</sub> nanotubes incorporated with CdS for photocatalytic hydrogen production from splitting water under visible light irradiation. *Int. J. Hydrogen Energy* **2010**, *35*, 7073–7079. [[CrossRef](#)]
143. Zhang, Y.J.; Yan, W.; Wu, Y.P.; Wang, Z.H. Synthesis of TiO<sub>2</sub> nanotubes coupled with CdS nanoparticles and production of hydrogen by photocatalytic water decomposition. *Mater. Lett.* **2008**, *62*, 3846–3848. [[CrossRef](#)]
144. Chandra, M.; Bhunia, K.; Pradhan, D. Controlled Synthesis of CuS/TiO<sub>2</sub> Heterostructured Nanocomposites for Enhanced Photocatalytic Hydrogen Generation through Water Splitting. *Inorg. Chem.* **2018**, *57*, 4524–4533. [[CrossRef](#)]
145. Dang, H.; Cheng, Z.; Yang, W.; Chen, W.; Huang, W.; Li, B.; Shi, Z.; Qiu, Y.; Dong, X.; Fan, H. Room-temperature synthesis of Cu<sub>x</sub>S (x = 1 or 2) co-modified TiO<sub>2</sub> nanocomposite and its highly efficient photocatalytic H<sub>2</sub> production activity. *J. Alloys Compd.* **2017**, *709*, 422–430. [[CrossRef](#)]
146. Wang, Q.; Huang, J.; Sun, H.; Ng, Y.H.; Zhang, K.Q.; Lai, Y. MoS<sub>2</sub> Quantum Dots@TiO<sub>2</sub> Nanotube Arrays: An Extended-Spectrum-Driven Photocatalyst for Solar Hydrogen Evolution. *ChemSusChem* **2018**, *11*, 1708–1721. [[CrossRef](#)] [[PubMed](#)]
147. Ng, B.J.; Putri, L.K.; Tan, L.L.; Pasbakhsh, P.; Chai, S.P. All-solid-state Z-scheme photocatalyst with carbon nanotubes as an electron mediator for hydrogen evolution under simulated solar light. *Chem. Eng. J.* **2017**, *316*, 41–49. [[CrossRef](#)]
148. Yang, C.; Qin, J.; Rajendran, S.; Zhang, X.; Liu, R. WS<sub>2</sub> and C-TiO<sub>2</sub> Nanorods Acting as Effective Charge Separators on g-C<sub>3</sub>N<sub>4</sub> to Boost Visible-Light Activated Hydrogen Production from Seawater. *ChemSusChem* **2018**, *11*, 4077–4085. [[CrossRef](#)] [[PubMed](#)]
149. Liu, E.; Xu, C.; Jin, C.; Fan, J.; Hu, X. Carbon quantum dots bridged TiO<sub>2</sub> and Cd<sub>0.5</sub>Zn<sub>0.5</sub>S film as solid-state Z-scheme photocatalyst with enhanced H<sub>2</sub> evolution activity. *J. Taiwan Inst. Chem. Eng.* **2019**, *97*, 316–325. [[CrossRef](#)]
150. Zou, Y.; Shi, J.W.; Ma, D.; Fan, Z.; Niu, C.; Wang, L. Fabrication of g-C<sub>3</sub>N<sub>4</sub>/Au/C-TiO<sub>2</sub> Hollow Structures as Visible-Light-Driven Z-Scheme Photocatalysts with Enhanced Photocatalytic H<sub>2</sub> Evolution. *ChemCatChem* **2017**, *9*, 3752–3761. [[CrossRef](#)]
151. Yang, G.; Ding, H.; Chen, D.; Feng, J.; Hao, Q.; Zhu, Y. Construction of urchin-like ZnIn<sub>2</sub>S<sub>4</sub>-Au-TiO<sub>2</sub> heterostructure with enhanced activity for photocatalytic hydrogen evolution. *Appl. Catal. B Environ.* **2018**, *234*, 260–267. [[CrossRef](#)]
152. Zhang, L.; Huang, Y.; Dai, C.; Liang, Q.; Yang, P.; Yang, H.; Yan, J. Constructing ZnO/ZnCr<sub>2</sub>O<sub>4</sub>@TiO<sub>2</sub> -NTA Nanocomposite for Photovoltaic Conversion and Photocatalytic Hydrogen Evolution. *J. Electron. Mater.* **2019**, *48*, 1724–1729. [[CrossRef](#)]
153. Ke, X.; Zhang, J.; Dai, K.; Liang, C. Construction of fluorinated-TiO<sub>2</sub> nanosheets with exposed {001} facets/CdSe-DETA nanojunction for enhancing visible-light-driven photocatalytic H<sub>2</sub> evolution. *Ceram. Int.* **2020**, *46*, 866–876. [[CrossRef](#)]
154. Kim, Y.K.; Lim, S.K.; Park, H.; Hoffmann, M.R.; Kim, S. Trilayer CdS/carbon nanofiber (CNF) mat/Pt-TiO<sub>2</sub> composite structures for solar hydrogen production: Effects of CNF mat thickness. *Appl. Catal. B Environ.* **2016**, *196*, 216–222. [[CrossRef](#)]

155. Dai, K.; Lv, J.; Zhang, J.; Zhu, G.; Geng, L.; Liang, C. Efficient Visible-Light-Driven Splitting of Water into Hydrogen over Surface-Fluorinated Anatase TiO<sub>2</sub> Nanosheets with Exposed {001} Facets/Layered CdS-Diethylenetriamine Nanobelts. *ACS Sustain. Chem. Eng.* **2018**, *6*, 12817–12826. [[CrossRef](#)]
156. Yuan, W.; Zhang, Z.; Cui, X.; Liu, H.; Tai, C.; Song, Y. Fabrication of Hollow Mesoporous CdS@TiO<sub>2</sub>@Au Microspheres with High Photocatalytic Activity for Hydrogen Evolution from Water under Visible Light. *ACS Sustain. Chem. Eng.* **2018**, *6*, 13766–13777. [[CrossRef](#)]
157. Zhao, H.; Wu, M.; Liu, J.; Deng, Z.; Li, Y.; Su, B.L. Synergistic promotion of solar-driven H<sub>2</sub> generation by three-dimensionally ordered macroporous structured TiO<sub>2</sub>-Au-CdS ternary photocatalyst. *Appl. Catal. B Environ.* **2016**, *184*, 182–190. [[CrossRef](#)]
158. Wu, M.; Zhang, J.; Liu, C.; Gong, Y.; Wang, R.; He, B.; Wang, H. Rational Design and Fabrication of Noble-metal-free Ni<sub>x</sub>P Cocatalyst Embedded 3D N-TiO<sub>2</sub>/g-C<sub>3</sub>N<sub>4</sub> Heterojunctions with Enhanced Photocatalytic Hydrogen Evolution. *ChemCatChem* **2018**, *10*, 3069–3077. [[CrossRef](#)]
159. Sampath, S.; Sellappa, K. Visible-light-driven photocatalysts for hydrogen production by water splitting. *Energy Sources Part A Recover. Util. Environ. Eff.* **2020**, *42*, 719–729. [[CrossRef](#)]
160. Azam, M.U.; Tahir, M.; Umer, M.; Tahir, B.; Shehzad, N.; Siraj, M. In-situ synthesis of TiO<sub>2</sub>/La<sub>2</sub>O<sub>2</sub>CO<sub>3</sub>/rGO composite under acidic/basic treatment with La<sup>3+</sup>/Ti<sup>3+</sup> as mediators for boosting photocatalytic H<sub>2</sub> evolution. *Int. J. Hydrogen Energy.* **2019**, *44*, 23669–23688. [[CrossRef](#)]
161. Zhu, J.; Zhang, M.; Xiong, J.; Yan, Y.; Li, W.; Cheng, G. Electrostatically assembled construction of ternary TiO<sub>2</sub>-Cu@C hybrid with enhanced solar-to-hydrogen evolution employing amorphous carbon dots as electronic mediator. *Chem. Eng. J.* **2019**, *375*, 121902. [[CrossRef](#)]



© 2020 by the authors. Licensee MDPI, Basel, Switzerland. This article is an open access article distributed under the terms and conditions of the Creative Commons Attribution (CC BY) license (<http://creativecommons.org/licenses/by/4.0/>).